Pre-Doctoral Research Year report

July 15, 2020

Optical transport of ultracold atoms

Student :

Damien Bloch
ENS Paris - Saclay,
4, avenue des Sciences,
Gif-sur-Yvette, 91190

Supervisor :

Dr. Ulrich Schneider
Many-body Quantum Dynamics,
Cavendish Laboratory,
JJ Thomson Avenue,
Cambridge

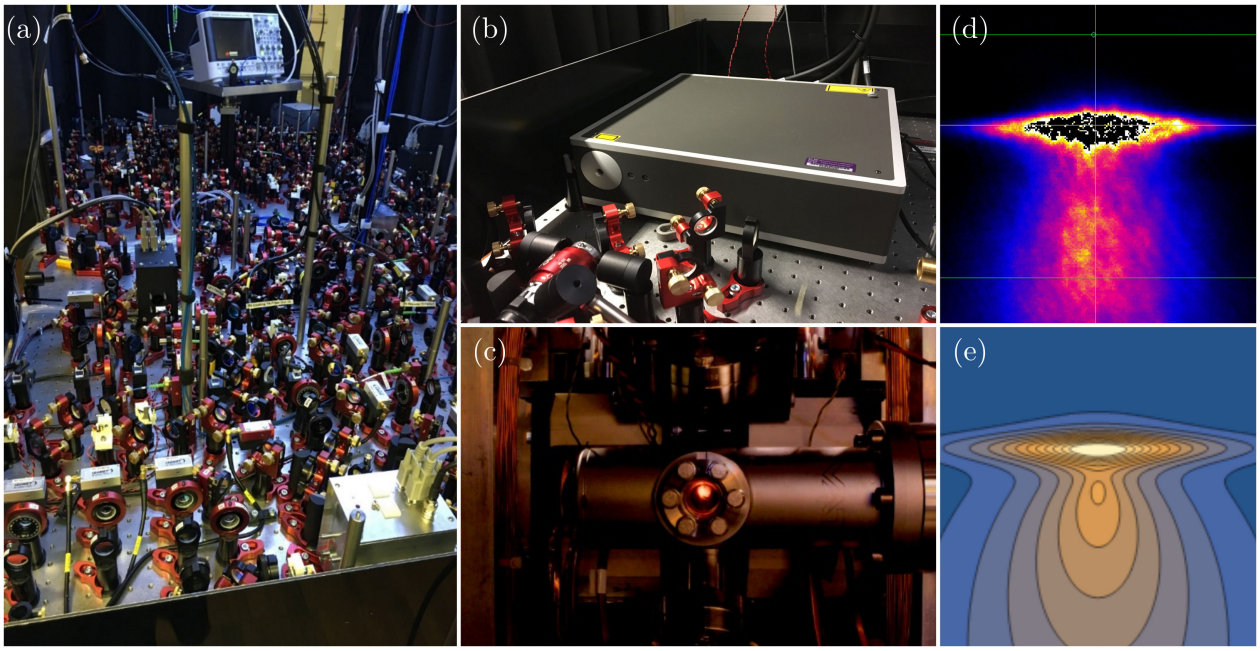

Figure 1: (a) Optical table for preparation and control of the lasers. (b) High power laser. (c) Fluorescence of an atomic cloud. (d,e) Hot atomic cloud falling from the magnetic trap.

Contents

Abstract

This thesis presents the work I did during my *Année de Recherche Pré-doctorale à l'Étranger* as part of my studies at the *École Normale Supérieure Paris-Saclay*. I worked in the Many-Body Quantum Dynamics (MBQD) group in the Cavendish Lab in Cambridge under the supervision of Dr. Ulrich Schneider.

One of the step of the experiment performed in the MBQD group is to load an ultracold atomic gas in a dipole trap. The trap position is then displaced over a macroscopic distance using a focus tunable lens. The aim of my project was to build and test a protocol of this transport scheme on the experiment.

During the internship, I first realised a prototype of this setup with a low power laser. Once it was demonstrated to behave as expected, I tested it with a high power laser. Eventually, I mounted the scheme on the experiment and first tests with cold atoms were performed.

A brief introduction explains the motivation to study the Kagome lattice with cold atoms. It is followed by a discussion of the tools used for the experiment and a description of the setup, with emphasis on the step of optical transport. The implementation of optical transport for this experiment is then detailed. Following this, is a theoretical justification of the viability and performances of the scheme.

Acknowledgements

I would like to thank Dr. Ulrich for the opportunity to work on an experiment that repetitively awed me by its size and ingenuity every time I learned a new fact about it. Also, particular thanks to the people in the MBQD group for making me feel welcome, especially for Luca Donini, Dr. Tiffany Harte, Max Melchner and Dan Reed who showed me the ropes of working in the lab. I also specially acknowledge Stephen Topliss, electronics technician in the Cavendish Lab, for the time he spent making a schematic on paper become an actual device.

1 Introduction

1.1 Quantum simulation

Predicting the behaviour of large interacting quantum systems is reputed to be a challenging task for all but the simplest problems. Simulations with classical computers provide insights, but are quickly limited by the exponential scaling of the Hilbert space with the size of the system. As of today, only calculations with a few tens of particles are tractable using this method, which is far from any macroscopic number.

One famous solution to circumvent this problem was made by Feynman [Fey82] : instead of considering the real problem, it might prove useful to extract its main features and engineer a toy quantum system sharing these same properties. The new model must be easier to observe while still being able to reproduce the expected behaviour of the original system. This point of view leads to two possibilities : quantum computers — which replace classical bits by quantum qubits — and analogue quantum simulations — which aim to reproduce Hamiltonians with continuous properties —.

The latter approach is exactly what is done in the field of cold atoms in order to replicate the comportment of electrons in solids by using instead atoms in optical lattices.

1.1.1 Lattice hamiltonians

A system of interacting electrons subjected to a periodic potential created by fixed ionic cores is believed to be well described by a *Hubbard Hamiltonian*. In the language of second quantisation, this is written as :

$$\widehat{H}_{FH} = -t \sum_{\substack{\langle i,j \rangle \\ \sigma \in \{\uparrow,\downarrow\}}} \hat{a}^\dagger_{i,\sigma}\, \hat{a}_{j,\sigma} + U \sum_i \hat{n}_{i,\uparrow}\, \hat{n}_{i,\downarrow} \tag{1}$$

Here $\hat{a}^\dagger_{i,\sigma}$ is the creation operator for a fermion on a lattice site i and a spin $\sigma \in \{\uparrow,\downarrow\}$. $\hat{n}_{i,\sigma} = \hat{a}^\dagger_{i,\sigma}\hat{a}_{i,\sigma}$ is the occupation number on site i. $\widehat{H}_{FH}$ is known as the *Fermi-Hubbard Hamiltonian* and describes how particles hop between lattice sites $\langle i,j \rangle$ with a rate t and with on-site interaction energy cost U when two fermions of opposite spin occupy the same site. The Hubbard model is only a crude approximation to a solid-state lattice model as it neglects some effects such as phononic excitations, long-range interactions or lattice defects. But even this simplified model presents a large phenomenology, with magnetic and metallic phase transitions.

It is worth noting that a similar Hamiltonian exists for bosons as well :

$$\widehat{H}_{BH} = -t \sum_{\langle i,j \rangle} \hat{b}^\dagger_i\, \hat{b}_j + \frac{U}{2} \sum_i \hat{n}_i(\hat{n}_i - 1) \tag{2}$$

with analogous definitions for the creation operators $\hat{b}^\dagger_i$ for bosons. This *Bose-Hubbard Hamiltonian* is a departure from solid state physics which involves fermionic electrons , but presents the same complexity than the Fermi-Hubbard Hamiltonian.

While it is possible to write down these Hamiltonians from first principles, diagonalising them for a given lattice geometry (*i.e.* a set of adjacent sites $\langle i,j \rangle$), is out of reach for large systems. The complexity of the previous models makes it difficult to gain insights on some phenomena just by looking at the Hamiltonians. Experimental data might prove especially useful to gain some

understanding. For solid state materials, it is an extremely difficult task to change the lattice geometry, the doping or the interaction strength. This is why another solution must be found in order to explore the space of parameters.

1.1.2 Cold atoms in optical lattices

This is where cold atoms are particularly useful because it is now possible to reproduce the behaviour of such systems but with large tunability. The idea is to observe the comportement of a cloud of cold atoms when they experience a periodic potential created by a standing light wave (see fig. 2). This new system can be made to follow the Hamiltonians described previously and a variety of tools have been developed to change the parameters at will [JZ05].

However, reaching quantum degeneracy with cold atoms is not a trivial task. But it must be achieved in order to simulate condensed matter in which the electrons are highly degenerate (*i.e.* their temperature is well below the Fermi temperature). The criteria characterising quantum degeneracy is the phase-space density :

$$\varpi = n_0 {\lambda_T}^3 \tag{3}$$

were n_0 is the peak density of particles and $\lambda_T = \sqrt{\frac{2\pi\hbar^2}{mk_BT}}$ is the thermal de Broglie wavelength. The system exhibits quantum properties when the wavelength of the particles is large enough to overlap with the neighbouring particles, *i.e.* when $n_0 {\lambda_T}^3 > 1$.

The developement of cold atoms techniques in the 1990s hit a milestone with the realisation of the first Bose-Einstein Condensate (BEC) [AEM+95]. In this state of matter, a large number of bosons condense into the ground state, displaying a macroscopic wavefunction. This success was shortly followed by the achievement of quantum degeneracy for fermions [DJ99]. It is now possible to routinely produce quantum systems and to study the behaviour of degenerate atomic clouds in non-trivial optical potentials.

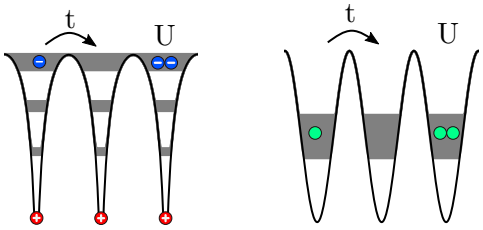

Electrons in potential created by ions

Atoms in standing wave potential

Figure 2: Illustration of the analogy between solid state and cold atoms.

	Electrons in solid	**Atoms in optical lattice**
Number	10^{24}	10^{6}
Timescale	10^{-15} s	10^{-2} s
Lifetime	∞	10 s
Lattice spacing	10^{-10} m	10^{-7} m
Possible imaging	X-rays diffraction	Optical microscope

Table 1: Comparison of parameters for solid state and cold atoms.

A major advantage of this technique over solid state physics is the different scale. The system is larger and its dynamics happens on a slower timescale (see table 1). Thanks to this, it is possible to directly probe the dynamical properties. Letting the cloud expand freely according to its inital speed with *time-of-flight measurement* allows to map the momentum distribution of the cloud. State-of-the art microscopy even allows to image the position of individual atoms in the

lattice [BGP+09].

Thanks to all these reasons, cold atoms physisc has proven to be a successful quantum simulation method and has been able to correctly predict a number of low temperature phenomena [Blo05].

1.2 Kagome lattice

Among all the possible lattice geometries, one is of particular interest : the Kagome lattice. Its geometry consists of corner sharing triangles as depicted in figure 3a. The aim of the experiment in the Many-Body Quantum Dynamics group (MBQD) in Cambridge is to implement this lattice with cold atoms.

The Kagome lattice is the next logical step after the triangular and honeycomb lattices. Its realisation is still ongoing and not all experimental difficulties have been overcome [JGT+12]. The interesting properties of this lattice come from its geometrical frustration that results in non-trivial ground states for the Hubbard Hamiltonians.

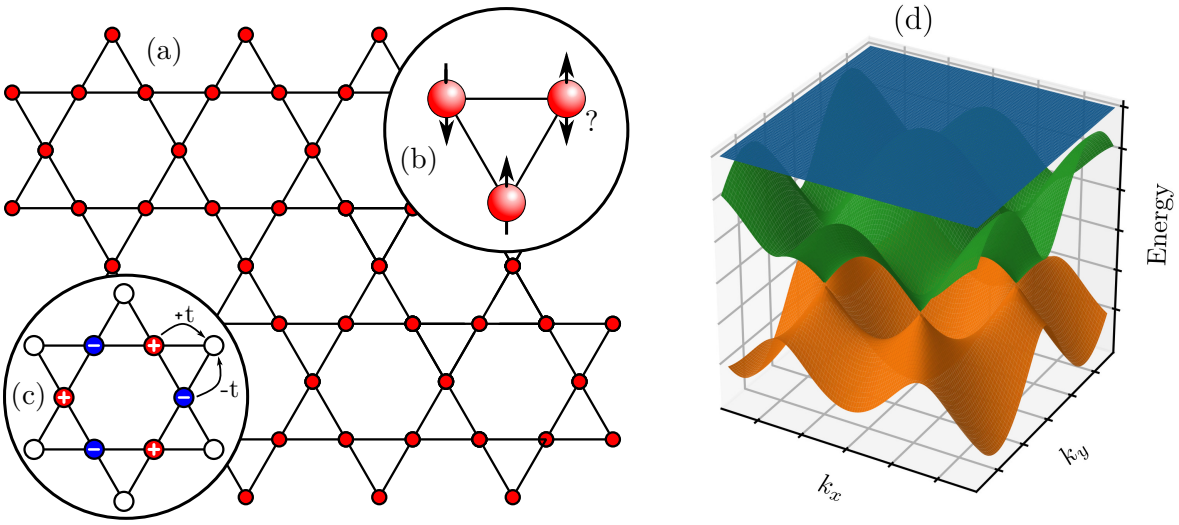

Figure 3: (a) Geometry of the Kagome lattice. (b) Spin frustration for the Kagome anti-ferromagnet. (c) Localized hexagonal eigenstate for a single particle. (d) Kagome band structure.

For example, the ground state of the Kagome anti-ferromagnet is still unknown. In this case, there is one atom per site and the energy is minimised with anti-parallel spins between nearest neighbours. But, even for one triangular cell, it is not possible to satisfy this criteria for all pairs of nearest neigbours (fig. 3b). Because of that, there is no energy cost required to flip a spin and the ground state of the triangular subcell is 6-fold degenerate. This degeneracy grows exponentially when more triangular cells are connected. This macroscopic degeneracy explains why the ground state of the Kagome anti-ferromagnet is hard to predict. It is speculated to be a novel type of spin state known as a *spin liquid* : a highly entangled state with long range correlations [YHW11]. Observing this state is one of the objectives of the experiment.

The Kagome frustration also reveals itself when looking at single particle eigenstates of the lattice. Indeed, it is possible to construct eigenstates on a hexagonal plaquette with alternating signs for the wavefunction as shown in figure 3c. While this is an eigenstate for a single particle on

the whole lattice, it is actually localized because the tunnelling cancels out for sites outside of the hexagon. Therefore the particle cannot move and has no kinetic energy. In other words, it means that one of the energy bands of the Kagome lattice is flat, as is illustrated in figure 3d. An explicit calculation of the band structure is done in appendix A.

Because the upper band is flat, the dynamics of particles in this state will be dominated by interactions as there is no other energy scale. As a result the ground state of the repulsive bosonic Kagome lattice is also exotic. Indeed, at high filling, it is predicted that the ground state will be formed of non-overlapping hexagons arranged on a grid, with particles condensing in the interstitial space [HA10]. This state of matter presents properties of both a solid and a BEC and is called a *supersolid*, which is currently under high investigation [LLH+17, LMZ+17]. If the Kagome lattice indeed presents a supersolid state, a realisation of it with cold atoms would be a direct proof of its existence and would allow to characterise this state.

2 Experimental setup

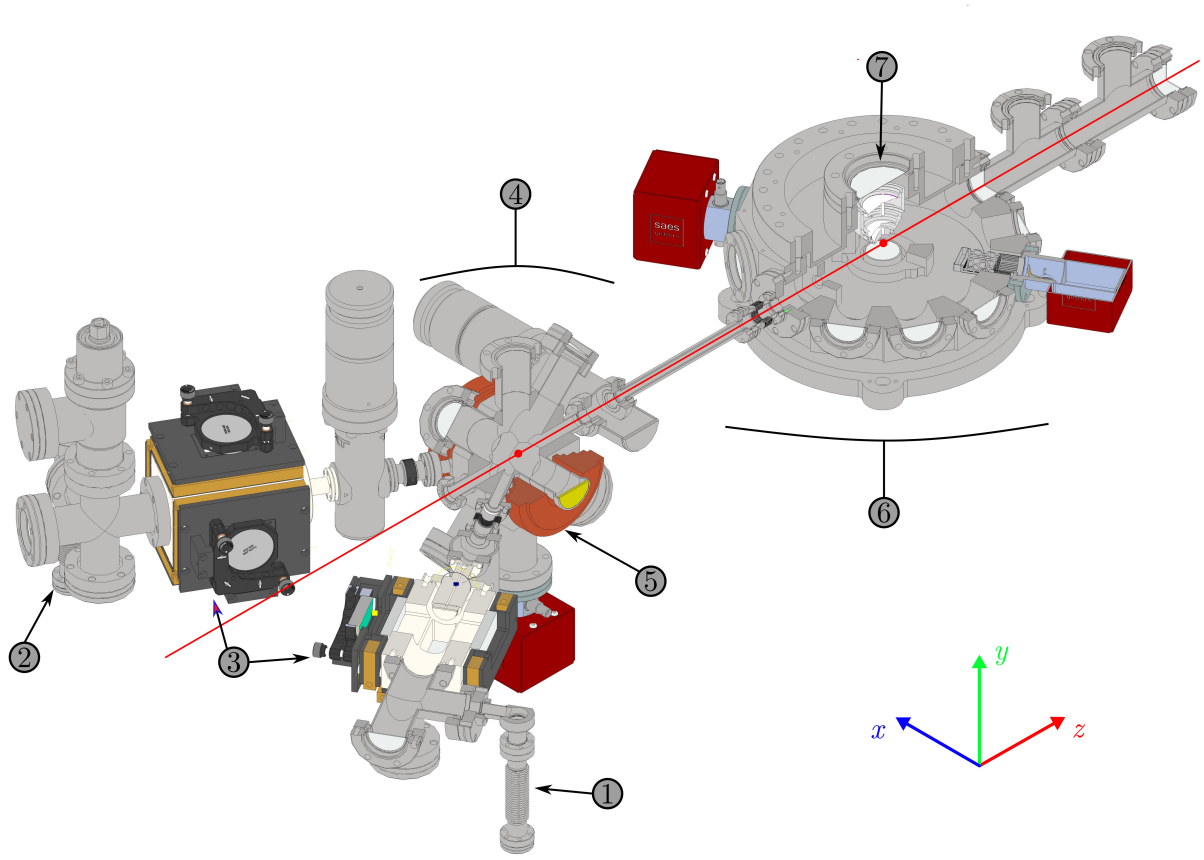

Figure 4: Experimental setup. (1) ^{87}Rb oven. (2) ^{39}K and ^{40}K oven. (3) 2D MOTs. (4) Cooling chamber (3D MOT + molasses + magnetic trap). (5) MOT & magnetic trap coils. (6) Science chamber. (7) Microscope. Highlighted in red is the transport axis with its start and end points. The science chamber is under construction and is not yet implemented.

Realising an optical Kagome lattice is the main goal of the experiment in the MBQD group and is a challenge in itself. But before being able to load atoms in the lattice it is necessary to reach quantum degeneracy by increasing the density of the gas cloud and reducing its temperature.

This is a major part of the experiment and the cooling section is already built with the science chamber to be added soon. Figure 4 is an illustration of the experimental setup and figure 5 shows the evolution of the phase space density at different points. They will be used as a roadmap for this section which is a description of the experimental techniques, with an emphasis on the steps where optical transport is involved.

More detailed descriptions of the techniques used to manipulate cold atoms can be found in [Foo07] or [BML00].

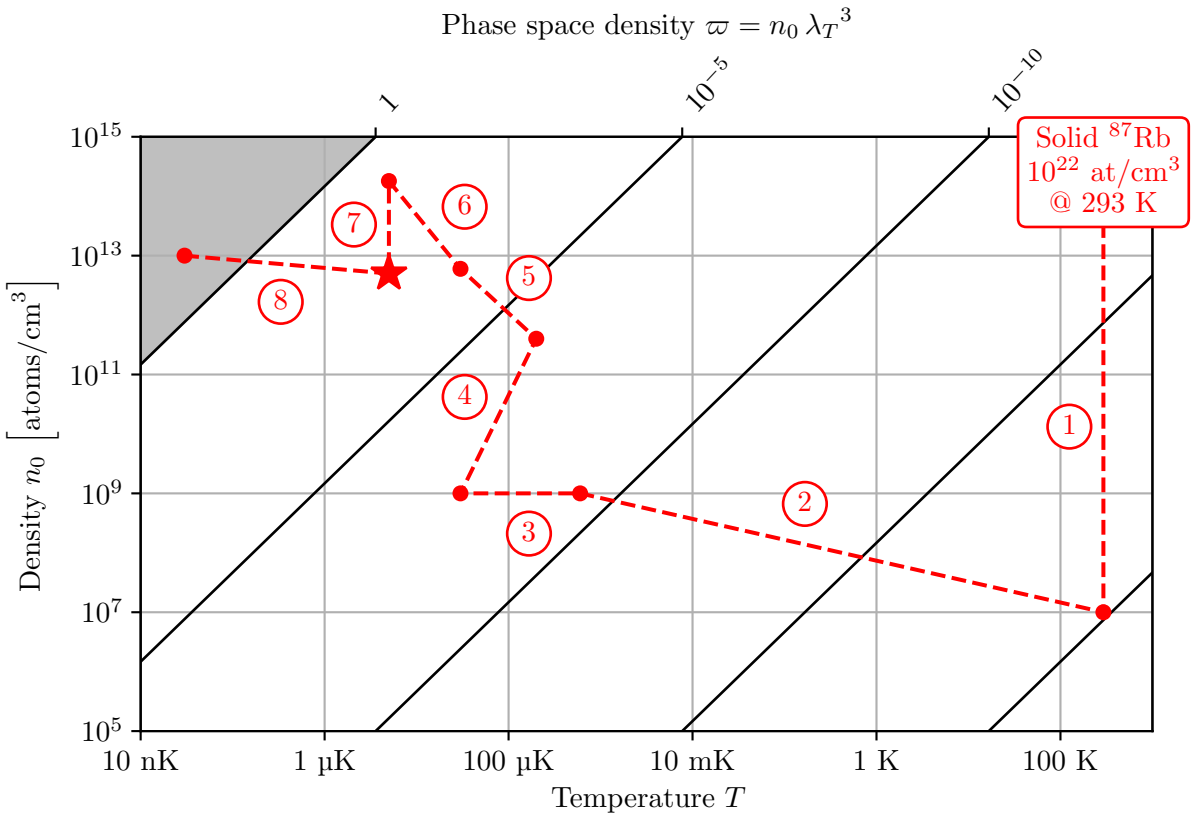

Figure 5: Phase space density at different points of the experiment (typical values). The grey area indicates the region of quantum degeneracy. (1) Sublimation of solid ^{87}Rb to the vapour phase. (2) Cooling in the MOT. (3) Sisyphus cooling. (4) Loading in the magnetic trap. (5) Microwave evaporation in the magnetic trap. (6) Evaporation in the hybrid trap. (7) Loading in the transport beam. (8) Evaporation in crossed dipole trap. ($\star$) Optical transport occurs at the star shaped point and without change in atom number or temperature.

2.1 Magneto-Optical Trap

2.1.1 Doppler cooling

Magneto-Optical Traps (MOT) are the workhorse of cold atom experiments [Foo07]. They are used to cool and trap an atomic vapour. The initial gas is typically produced by evaporating a solid

sample under high vacuum.

When atoms in this vapour are illuminated by a resonant laser, they can absorb an incoming photon and reemit it in a random direction. On average, for many absorption-emission cycles, atoms will feel a force in the direction opposed to to the propagation of the laser beam. In a MOT, the laser is slightly detuned below the atomic transition to make use of the Doppler effect. With this, stationary particles do not interact with the light, but the atoms moving in the direction of the laser see photons of higher frequency, closer to resonance, and are indeed slowed down. When combining counter-propagating beams in all three directions, this produces a viscous force in opposition to the velocity of the atoms.

The lasers effectively cool down the atomic cloud, but don't provide confinement on their own. A position-dependent force is added in the presence of an inhomogeneous magnetic field. In this configuration, the magnetic field induces a Zeeman shift that depends on the position of the atoms and it is possible to trap the cloud in a given area in space.

For the actual implementation in the considered experiment, the atomic vapour is first cooled down only in the transverse plane when going through a 2D MOT. The slowed flux of atoms is then used to load a 3D MOT in the cooling chamber. Even if the force felt by the atoms is on average null in a MOT, the constant absorption-reemission process creates a random walk in momentum space. Because of that, magneto-optical trapping is limited to temperatures above 150 µK for alkali species.

2.1.2 Sub-Doppler cooling

It is possible to go below this temperature when only using the lasers of the MOT. The counter-propagating beams can be tuned to form an interference pattern. This leads to a cooling mechanism called *Sisyphus cooling* : the atoms repeatedly climb to the top of the potential barrier created by the optical Stark effect of the interfering laser beams, and then suddenly drop to the bottom of the potential well after absorption and emission of a photon. The energy loss in this process is taken from the atom's thermal energy. This step allows to reach even lower temperature, but it is still not enough to reach the quantum regime.

2.2 Magnetic trap

2.2.1 Magnetic trapping

In order to reduce the temperature even more, the atoms are transferred in a magnetic trap were they will undergo evaporation. This kind of trap provides a lifetime of several seconds and is the last cooling step before transferring the atoms to the science chamber.

The technique relies on the interaction of an atom's magnetic moment $\boldsymbol{\mu}$ with an external field field $\mathbf{B}$, yielding a potential energy :

$$U(\mathbf{r}) = -\boldsymbol{\mu} \cdot \mathbf{B}(\mathbf{r}) \tag{4}$$

The magnetic moment is proportional to the total angular momentum $\mathbf{F}$ of the atom and when projecting onto the quantisation axis defined by the magnetic field, one obtains :

$$U(\mathbf{r}) = g_F m_F \mu_B B(\mathbf{r}) \tag{5}$$

where μ_B is the Bohr magneton, g_F is the Landé, factor which depends on the atomic state, and m_F is the projection of the angular momentum onto the magnetic field.

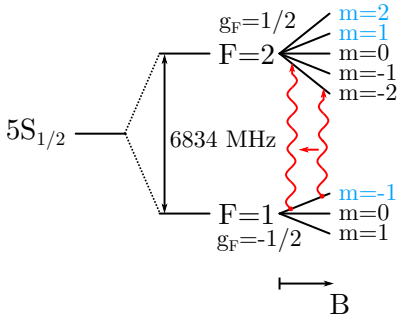

Figure 6: Zeeman shift for the lower energy levels of ^{87}Rb with increasing magnetic field. In blue are low-field seeking states. The red arrows indicate the microwave sweep for evaporation.

The atoms acquire a potential energy proportional to the magnitude of the magnetic field. Depending on the sign of the proportionality constant $g_F m_F$, atoms are either attracted by the maximum or minimum of the magnetic field (see fig. 6). In practice it is only possible to realise a minimum of magnetic field in free space, so only the latter case of *low-field seeking* atoms is interesting for trapping. This requires the atoms to be polarised in a correct spin state (here $F = 1$, $m_F = -1$) before being loaded in the trap.

In the experiment, the magnetic trap is realised by using the MOT coils in an anti-Helmholtz configuration. This creates a magnetic field that is indeed minimal in the center of the chamber and actually cancels :

$$\mathbf{B}(\mathbf{r}) = B' \left[x, \frac{y}{2}, \frac{z}{2}\right]^\top \tag{6}$$

Here B' is the magnetic field gradient that dictates the strength of the trap.

After the MOT step, the cloud is loaded in the magnetic trap by turning the lasers off and suddenly increasing the current in the coils. This compresses the cloud and causes it to heat up.

2.2.2 Microwave evaporation

Having a high density in space is useful for the next step of evaporation. The idea is to remove the hottest atoms from the trap. After thermalisation, the remaining atoms will have a lower temperature. But for this to be effective, it is necessary to have enough collisions between particles to allow for fast thermalisation.

Removing the hottest atoms is done by driving a microwave transition between the initially low-field seeking state to a high-field seeking state that will be expelled from the trap. The microwave knife is at first detuned below the fundamental transition between $F = 1$ and $F = 2$ such that only the atoms far from the center (*i.e.* the hot ones) are targeted (see fig. 6). The transition frequency is then increased closer to the zero-field transition to evaporate the cloud further.

2.2.3 Majorana losses

A major inconvenience with the anti-Helmholtz configuration is the issue of *Majorana losses*. This occurs when trapped atoms cross the zero magnetic field area. When the field is zero, there is no longer a well-defined quantisation axis. Any fluctuation or collision can cause the magnetic moment of the atom to be randomly changed. After traversing the zero field region, the atom can then possibly be in an untrapped state that is repelled from the trap center (see fig. 7a,b). This effect leads to both atoms loss and heating as the ejected atom can collide with other atoms on its way out.

At high enough temperature (>100 µK), this effect is not dramatic because the atoms are not likely to spend a lot of time in the zero field region, but it becomes troublesome when trying to reach quantum degeneracy. Indeed, when the cloud is cold and dense, its density will be high in the center of the magnetic trap.

The solution chosen to avoid this problem for the experiment will be described in the next paragraphs that discuss dipole trapping.

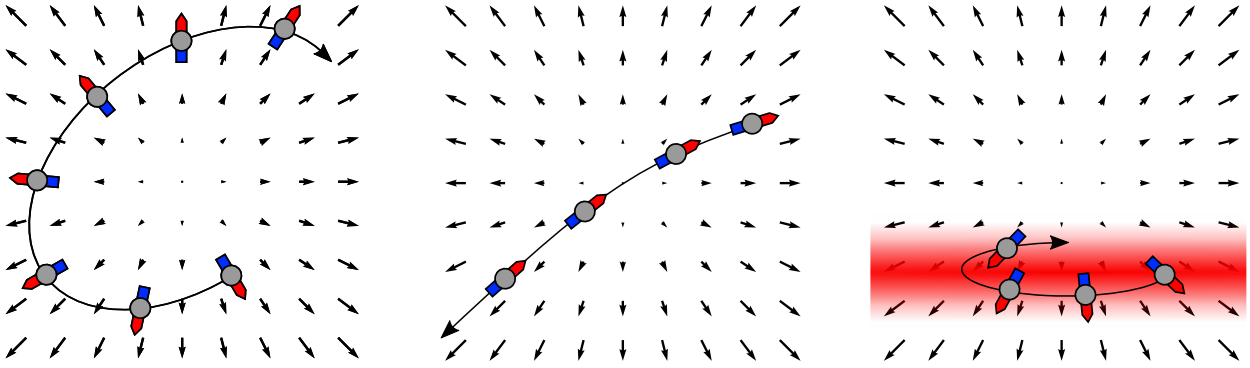

(a) Trapped atom with magnetic momentum aligned on the magnetic field.

(b) Initially trapped atom crossing the zero field area and ending up in an untrapped state.

(c) Trapped atom in the combination of magnetic and optical trap.

Figure 7: Illustration of the trapping mechanism in the magnetic trap.

2.3 Dipole trap

2.3.1 Dipole force

Once the atoms are at a low temperature, the preferred tool to manipulate them is with far detuned laser light ($\gtrapprox 5$ nm). It exercises a conservative force on the atoms while keeping a low scattering rate, thus minimizing heating.

This interaction, known as dipolar force, can be simply understood with a classical picture : in the presence of the electric field $\mathbf{E}$ of the laser, the electronic cloud is polarised, resulting in an induced dipole $\mathbf{p} = \alpha\mathbf{E}$. Here α is the atomic polarisability depending of the specie and the light wavelength. In the electric field, this dipole has a potential energy :

$$U = \mathbf{p} \cdot \mathbf{E} = \alpha |\mathbf{E}|^2 \tag{7}$$

The atom therefore feels a potential energy that is proportional to the light intensity $I = c\epsilon_0 |\mathbf{E}|^2/2$ at its position.

A rigourous way to describe the dipolar force is with time-dependent quantum perturbation theory. The interaction between far-detuned light and the atoms can then be understood as an AC Stark effect that shifts the electronic energy levels. When focusing on the ground state, its energy change is proportional to the light intensity experienced by the atom (see fig. 8). This is effectively equivalent to the classical picture, but provides an explicit expression for the dipolar force. A detailled derivation is provided in [GWO00]. The expression for the potential energy is then given by :

$$U(\mathbf{r}) = -\frac{3\pi c^2}{2\omega_0^3} \left(\frac{\Gamma}{\omega_0 - \omega} + \frac{\Gamma}{\omega_0 + \omega} \right) I(\mathbf{r}) \tag{8}$$

The atoms experience a potential energy that is proportional to the light intensity, with :

- $\Gamma \simeq 2\pi \times 6$ MHz, the width of the atomic transition[1]

[1] Typical value for potassium and rubidium.

- $\omega_0 \simeq 2\pi c/(780\ nm)$, the frequency of the transition[2]
- ω, the frequency of the light used to realise the trap

An interesting property of the prefactor before the intensity, is that its sign changes with the sign of the detuning $\omega_0 - \omega$. Therefore for *red-detuned light*, where the wavelength of the laser is larger than the wavelength of the atomic transition, the atoms are attracted to the area of high intensity. This is the inverse for *blue-detuned light* where particles are repulsed by larger intensity.

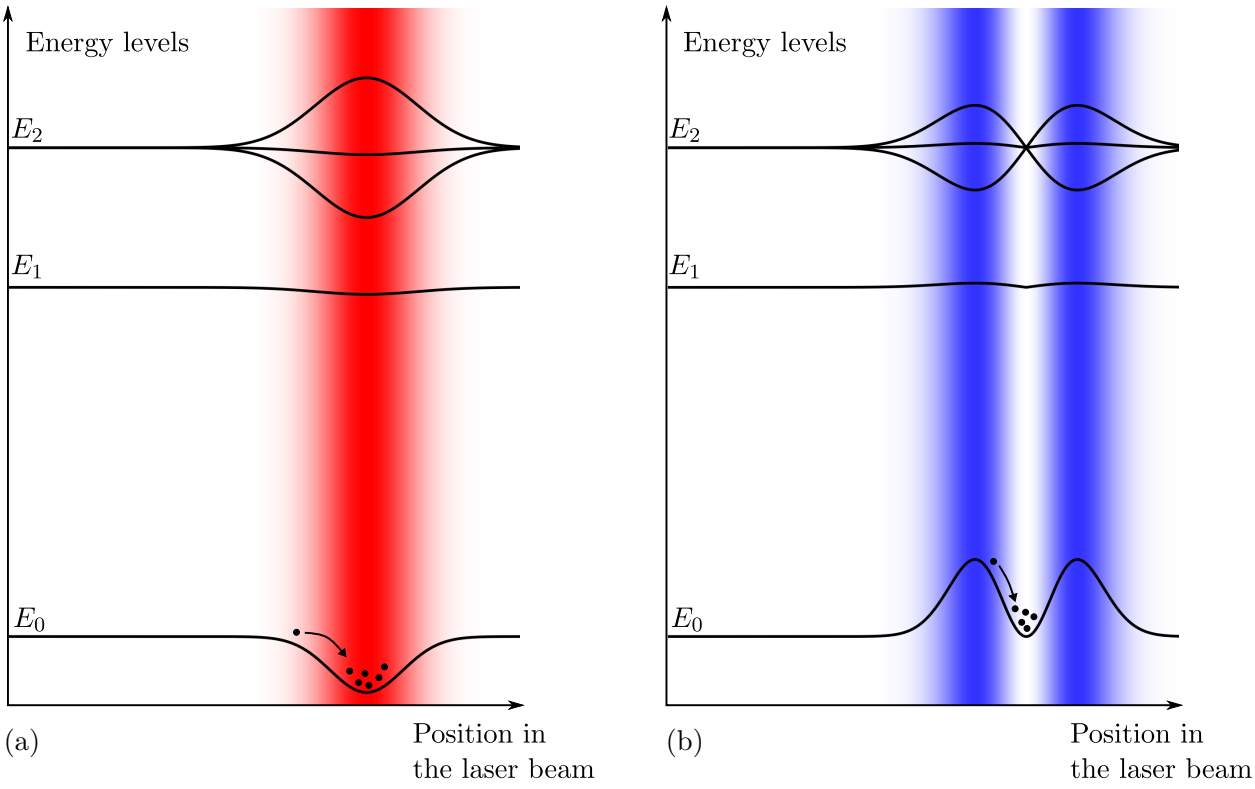

Figure 8: Illustration of far-detuned dipole trap. (a) Red detuned trap. (b) Blue detuned trap.

When the wavelength of the light is far enough (tens of nanometres) from the atomic transition, the rate Γ for of photon to be scatted by the atom is low :

$$\Gamma \propto \frac{I}{(\omega_0 - \omega)^2} \tag{9}$$

The atomic cloud can be trapped in the conservative potential for several seconds without heating. One limitation that comes from being far from resonance is that a high power laser (typically several Watts) is required to have acceptable trap depth.

Still, the characteristics of the interaction between far-detuned light and atoms make it a particularly suitable tool to manipulate ultracold clouds. This is the preferred option for the last steps of the experiment.

[2]For alkali species, this expression must be summed for the D_1 and D_2 lines with respective weights 1/3 and 2/3. This has little influence on the potential for detuning much larger than the fine structure.

2.3.2 Transport trap

The simplest way to build an optical trap using the dipole force is to focalise a gaussian red-detuned laser beam at a position in space (see fig. 9). The atomic cloud will then be attracted at the point where the light intensity is maximal.

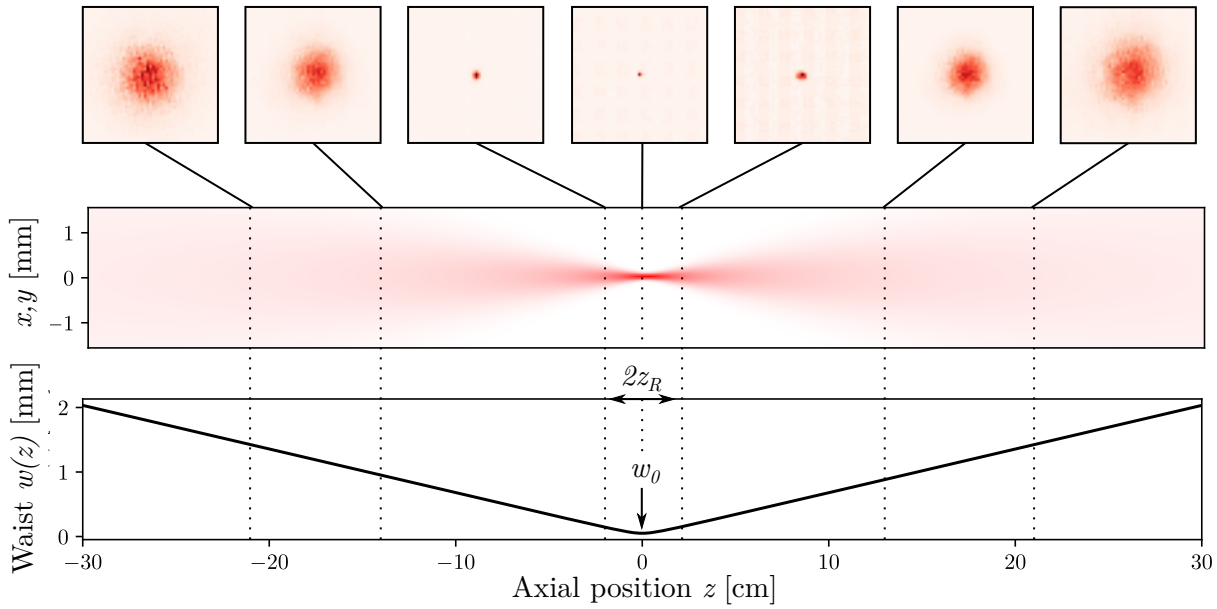

Figure 9: Gaussian beam profile used for optical transport and evolution of its waist.

A gaussian beam is the standard intensity profile that is obtained for example at the output of a single-mode fibre. In every transverse plane, the intensity will have a gaussian shape with a size evolving along the optical axis. The intensity profile for such a beam is (see [Sie86]) :

$$I(\mathbf{r}) = \frac{2P}{\pi w(z)^2} \exp\left(-2\frac{x^2+y^2}{w(z)^2}\right) \tag{10}$$

Here z is the optical axis and x, y are transverse coordinates. P is the power of the laser. $w(z)$ is the spot size of the beam, with a minimal waist value w_0 at the focal point $z = 0$. The waist is given by :

$$w(z) = w_0\sqrt{1+\left(\frac{z}{z_R}\right)^2} \tag{11}$$

In this expression z_R is the Rayleigh length, characterizing the distance after which the beam starts to diverge :

$$z_R = \frac{\pi {w_0}^2}{\lambda} \tag{12}$$

Using equation 8, the potential energy of the atom in the light field can be computed. It forms a well of finite depth with a strong confinement in the transverse direction, and a much weaker confinement along the optical axis (see fig. 10a).

Near the trap bottom, the potential can be approximated by a harmonic oscillator :

$$U(\mathbf{r}) \simeq -U_0 + \frac{m{\omega_x}^2 x^2}{2} + \frac{m{\omega_y}^2 y^2}{2} + \frac{m{\omega_z}^2 z^2}{2} \quad \text{for } x, y \ll w_0 \text{ and } z \ll z_R \tag{13}$$

The main properties of the transport trap are summarized in table 2

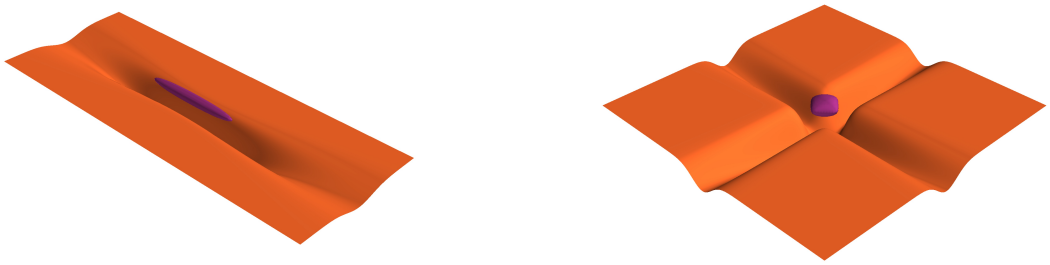

(a) Transport trap (b) Crossed trap

Figure 10: Illustration of the geometries for optical dipole traps. In orange is a sheet of the potential well and in purple is the shape of the atomic cloud.

.

Laser wavelength	λ	1064 nm
Laser power	P	5 W
Waist	w_0	50 µm
Rayleigh length	$z_R = \frac{\pi {w_0}^2}{\lambda}$	7.4 mm
Trap depth	$U_0 = \frac{3Pc^2}{{\omega_0}^3 {w_0}^2}\left(\frac{\Gamma}{\omega_0-\omega} + \frac{\Gamma}{\omega_0+\omega}\right)$	$k_B \times$ 195 µK
Transverse frequencies	$\omega_{x,y} = \sqrt{\frac{4U_0}{m{w_0}^2}}$	$2\pi \times$ 870 Hz
Axial frequency	$\omega_z = \sqrt{\frac{2U_0}{m{z_R}^2}}$	$2\pi \times$ 4.2 Hz
Transverse size at $T = 5$ µK	$\sigma_{x,y} = \sqrt{\frac{k_B T}{m{\omega_{x,y}}^2}}$	4 µm
Axial size at $T = 5$ µK	$\sigma_z = \sqrt{\frac{k_B T}{m{\omega_z}^2}}$	0.8 mm

Table 2: Transport trap parameters for ^{87}Rb.

While the transport trap is straightforward to realise with one laser beam, it does not provide a strong confinement along the beam direction. The cloud is therefore very elongated and diluted. Because of that, thermalisation time is long (tens of milliseconds) and the density is too low to achieve Bose-Einstein condensation.

This kind of trap is however useful in combination with the previously described magnetic trap, forming a *hybrid trap* [LPC+09]. The laser beam is overlapped with the magnetic trap such that the focal point of the laser is situated 50 µm below the center of the magnetic trap (see fig. 7c). With

this, the magnetic trap provides a good axial confinement while the laser beam assures transverse confinement and prevents the atoms from getting close the zero field region.

During the experiment, atoms are first evaporated in the magnetic trap and the transport beam is then turned on, forming this hybrid trap. Further evaporation can then be achieved. After this, the magnetic trap is adiabaticly turned off and the cloud is loaded in the transport beam and is free to expand in the axial direction.

The idea behind my project of optical transport, is to capture the cloud in this single beam trap. The position of the focal point, initially in the cooling chamber, is then progressively changed to be in the science chamber. The atoms will follow the maximum of intensity and be displaced. A detailed description of the transport scheme is reserved for the next sections.

2.3.3 Crossed dipole trap

Once the atoms have been transported to the science chamber, they need to undergo a last step of evaporation before reaching quantum degeneracy and forming a BEC. For this purpose, the atoms are trapped in a crossed optical dipole trap (XODT) which is the 90° combination of two gaussian beams similar to the transport laser (see fig. 10b). This geometry provides a tight confinement in all three directions of space. The density of the cloud is now high enough to allow thermalisation during evaporation. This is simply done by slowly reducing the power of the two crossed beams, thus reducing the trap depth. With this it is possible to reach the high density and low temperature necessary for Bose-Einstein condensation.

2.4 Lattice

Now that the atoms are in a degenerate quantum state, they are ready to be placed in the Kagome lattice. The lattice is also realised using the dipolar force. When several coherent laser beams overlap, an interference pattern is formed. Depending on whether the light is blue or red-detuned, atoms will be be attracted at the nodes or anti-nodes.

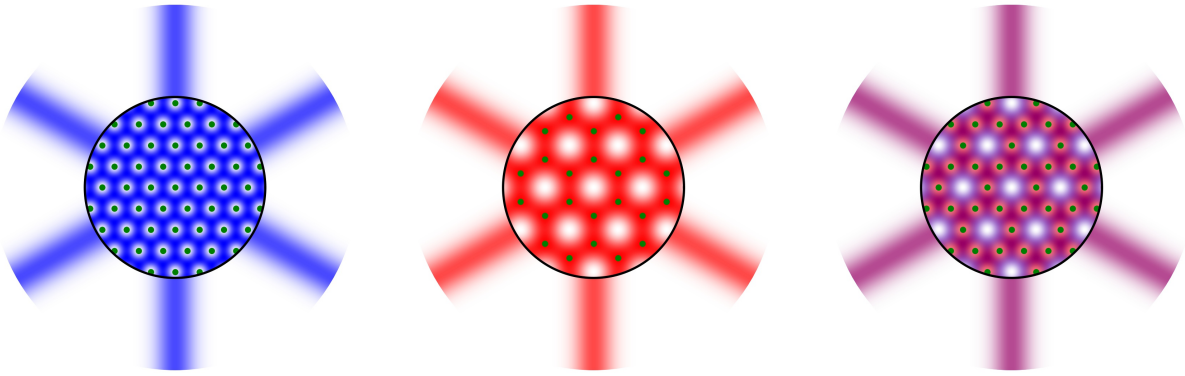

(a) Blue detunned triangular lattice.

(b) Red detunned honeycomb lattice.

(c) Kagome lattice resulting of the superposition of the two previous lattices.

Figure 11: Illustration of optical lattices. Green dots represent the atoms in the lattices.

Interfering three blue-detuned beams at 532 nm as in figure 11a will result in a triangular lattice with atoms trapped at the minimum of intensity. If the same is done for red-detuned lasers at

twice the wavelength (1064 nm), this will create a hexagonal lattice with a spacing two times larger (see fig. 11b).

Superposing the red-detuned lattice on the blue-detuned one will deepen 3 out of 4 sites of the blue triangular lattice and the final result is a Kagome lattice (see fig. 11c). This is how the Kagome geometry will be implemented. The actual realisation is more complicated than this simple picture, because the relative phases between the beams must be stabilised to prevent the lattice from moving.

With the atoms in the lattice, it will be possible to change several parameters (specie, number, temperature, lattice depth, interactions, ...) and to image atoms on single sites with an optical microscope. Having such a high control over the system will allow to answer some of the open questions for the behaviour of quantum particles in a Kagome lattice.

3 Transport implementation

3.1 Transport scheme

In the steps described above, my project to focus on optical transport and its implementation. It consists in trapping a cold atomic cloud at the focus of a red-detuned laser beam in the cooling chamber. The position of the focus is then progressively changed by $D = 50$ cm using a focus tunable lens. At the end of this step, the atoms are in the science chamber and the rest of the experiment is carried out.

Moving the atoms between two chambers allows to dedicate one to cooling and the other to the experiment itself. It provides better access for optical components around the chambers now that the two parts of the experiment are clearly separated. This is why transporting the cloud over a macroscopic distance is an usual step for most cold atoms experiments. There are several ways for doing this, but most of them rely on movable mirror on a moving rail, which is susceptible to failure after repeated use and generates vibrations close to the experiment.

The tunable lens scheme considered here doesn't suffer from these limitations. It is adapted from the demonstrating paper [LLM+14] and is illustrated in figure 12. It is a fairly simple technique with a small number of components besides the high power laser used. The tunable lens is used to dynamically change the divergence of a collimated beam. The fixed lens $f = 500$ mm focuses the beam on the atoms and is placed 500 mm after the tunable lens. The position of the fixed lens ensures that the trap waist is constant no matter the position to which the beam is focused (an explicit calculation using ABCD matrices is done in appendix B).

During the internship, I first realised a prototype of the scheme with a low power laser to ensure that it is indeed working as expected. Some results can be seen in figure 12 were the measured waists[3] are in good agreement with the predictions. The distance between the tunable lens and the fixed lens f was optimised to minimize the change of the waist w_0 during transport.

3.2 High power laser

Due to the large detuning between the laser used (1064 nm) and the atomic resonance (780 nm), a high intensity beam (5 W) is needed to create a trap with a depth of several hundreds microkelvins. The next step after the first prototype of optical transport was to prepare the high power beam used for transport (see fig. 13)[4].

[3] Measured by fitting a 2D gaussian picture.

[4] This was done with the help of Luca Donini, PHD student in the MBQD group.

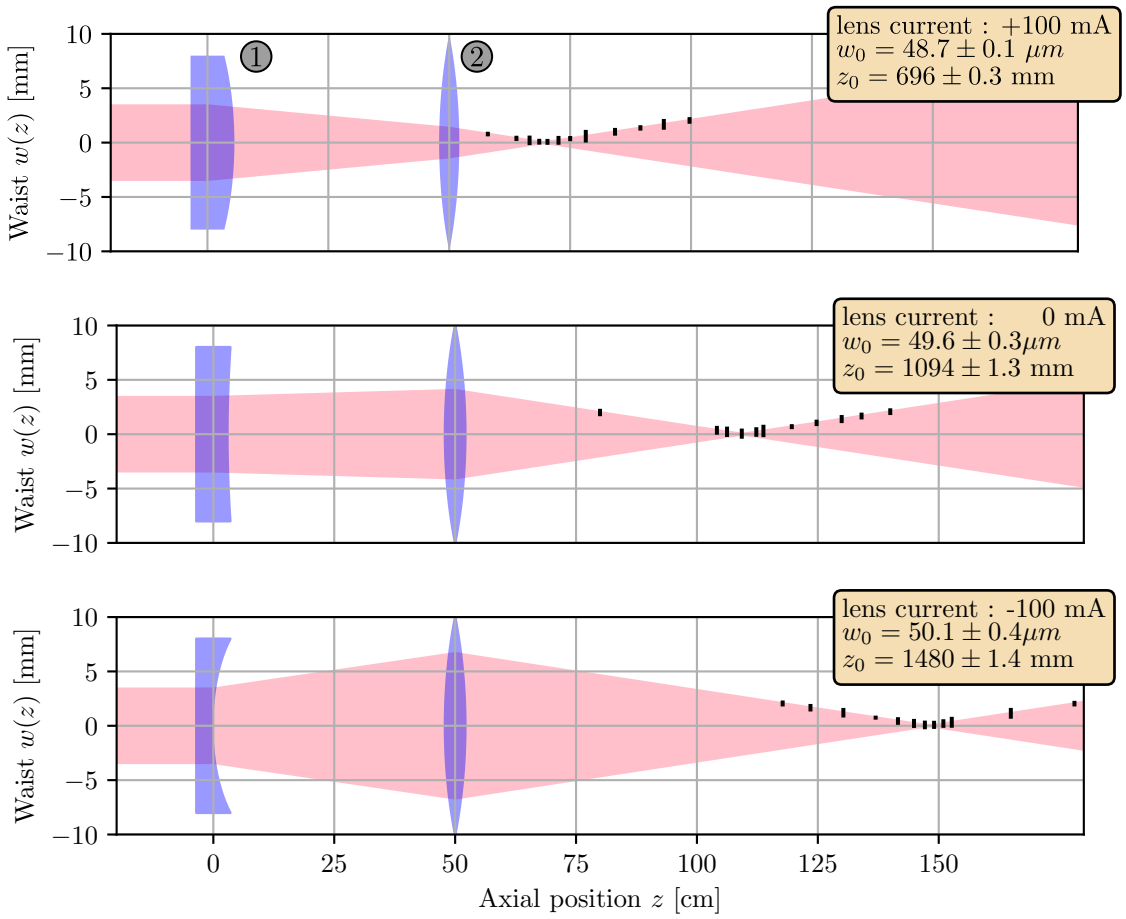

Figure 12: Illustration of the transport scheme. A tunable lens (1) is used to change the focus position of a collimated beam. A standard lens $f = 500$ mm (2) focuses the beam. The atomic cloud is trapped in the region of high intensity. The three figures correspond to different positions for the trap. The black bars are experimental measures used to determine the parameters of the beam.

The beam is produced by a commercially available Nd:YAG laser[5] delivering 42 W. After going through an optical isolator to protect the laser from back reflections, the beam is split in several paths with half-waveplates and polarising beam splitters. One path is for optical transport and the others are for the crossed dipole trap.

After going through an acousto-optic modulator (AOM), the beam is sent via optical fibre to the experiment table. An AOM operates by sending sound waves through a crystal. The laser traversing the crystal is diffracted into several beams when interacting with the density pattern created by the sound waves. By modulating the amplitude of the radio-frequency supplied to the AOM, it is possible to change the power going into each beam path. With this technique, it is possible to use the AOM as a shutter to turn on or off the laser.

The AOM is also used in coordination with a photodiode to keep the intensity of the light constant at the output of the fibre. A PID loop measures the power of the beam sent to the atoms and adjusts the signal of the AOM to keep this value constant. This precaution is important as any

[5]Coherent Mephisto MOPA 42

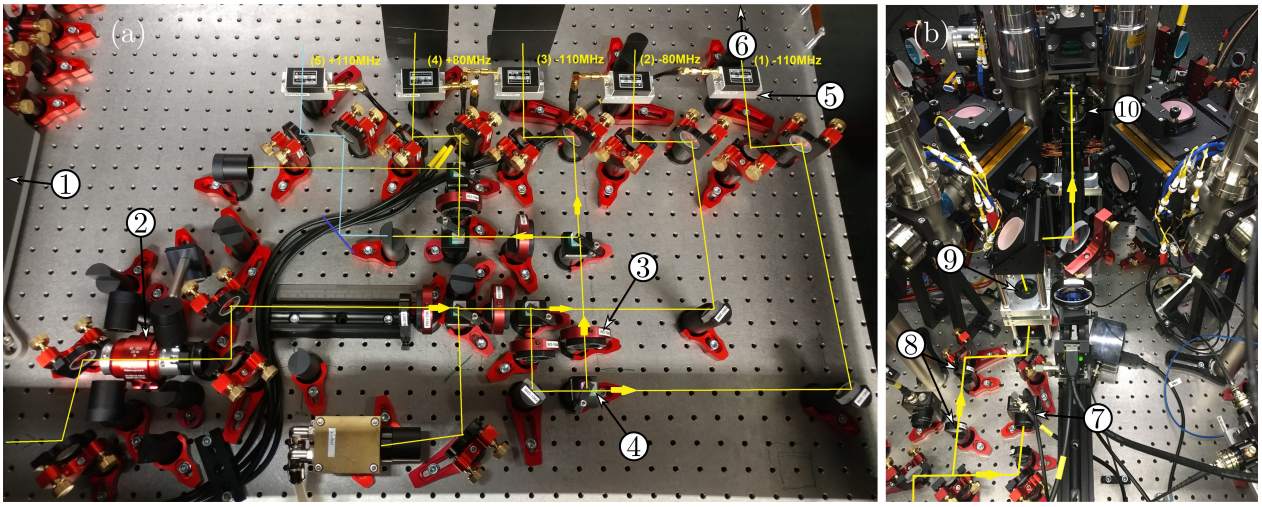

Figure 13: Pictures of the high power beam path built. (a) Preparation of the beam. (b) Experiment table. (1) Mephisto. (2) Optical isolator. (3) Half waveplate. (4) Beam splitters. (5) AOM. (6) To fibre. (7) Photodiode. (8) Telescope. (9) Tunable lens. (10) Focusing lens.

fluctuation in the light intensity will cause fluctuation of the trap depth and frequencies, resulting in an increase in temperature of the atoms [SOT97].

With this and a simple telescope to collimate the beam at the output of the fibre, the laser can be shone through the tunable[6] and fixed focusing lens and used to trap the atomic cloud.

3.3 Tunable lens

The key element for optical transport is the tunable lens. This component became commercially available a few years ago. While providing new flexibility, this technology is not as mature as other optical components and the tunable lens turned out to be the most sensitive part of this setup.

Figure 14: Tunable lens illustration.

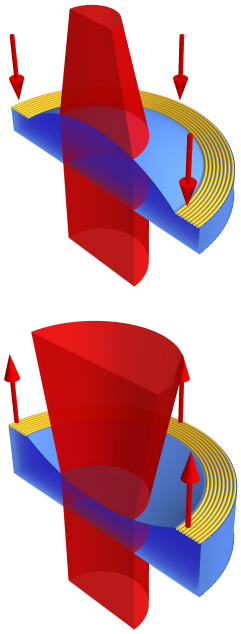

3.3.1 Working principle

The tunable lens[7] used on this experiment is made of an optical fluid held by a flexible polymer membrane (see fig. 14). A wire coil is fixed on the outer rim of the membrane. When a current is passed through the coil, it will be attracted (or repelled depending on the sign of the current) by a permanent magnet. The pressure exercised on the fluid inside the membrane will change the curvature of the lens. Therefore, it is possible to control the optical power of the lens[8] proportionally to the current in the coil.

The lens aperture is reasonably large (16 mm) and the focal power range can be controlled between -2 dpt to +3 dpt with a current of $\pm 200mA$. When converting the optical power to a position for the dipole trap, it gives more than one meter of change which is plenty in our case. The lens allows

[6] In the setup, the tunable lens must be placed horizontally. This is to prevent a gravity induced sag of the lens fluid that would distort the beam.

[7] Optotune EL-16-40-TC

[8] The optical power is the inverse of the focal length.

the trap center (*i.e.* the focal point) to be quickly (<50 ms) switched from the center of one chamber to the center of the other. However, that doesn't mean that transport is possible in this timescale and the limiting factor will be the inertia of the atoms : if the trap is abruptly switched from being in the cooling chamber to the science chamber, the cloud will simply stay behind and be lost.

3.3.2 Thermal dependance

The tunable lens is the one element that allows this setup to be compact and with no moving piece. However it is also a sensitive part and if no care is done to understand its properties, it can lead to poor transport performance.

One major trouble with the lens is that the focal length depends of the temperature of the fluid inside. Indeed, if the liquid is heated, it will expand, thus changing the lens curvature and its optical index. One could think that this effect is a small perturbation, but for transport it can cause the trap the be several centimetres away from the expected position.

A first issue related to thermal fluctuations was encountered during the initial tests of the lens. After several tens of minutes of use, the temperature of the lens rises up by several degrees. This is because the current in the coil dissipates about one Watt of power in the lens and the heat builds up over time. As a result, the lens is slowly and uniformly heated as show in figure 15b.

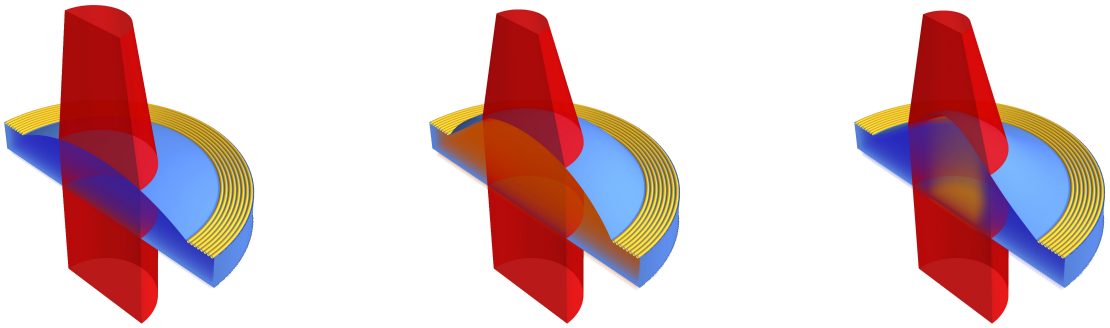

(a) Reference curvature of the lens in nominal conditions at room temperature and with low power light.

(b) Uniform heating of the lens liquid due to dissipation in the coil.

(c) Localised heating of the lens liquid due to absorption of the laser.

Figure 15: Influence of the temperature on the optical properties of the lens. This causes the focal length of the lens to fluctuate even at constant current.

Because of this effect, even if a constant current is applied to the lens, the trap position can fluctuates if the temperature is free to change. This effect is described in the lens datasheet and the manufacturer provides a way to correct this problem. Indeed, the lens shape remains spherical as the temperature changes and it just means that the optical power of the lens depends of two variables : the current in the coil and the temperature of the fluid. A sensor integrated in the lens allows to measure the temperature of the liquid.

We found that one possible way to fix the problem is to compensate the current of the coil as the temperature drifts. Instead of holding the current constant, its value is slightly tuned in order to negate the drift due to thermal dilatation. This solution requires to measure the influence of temperature on the optical power, but once this was done, it proved to be effective (see fig. 16). In addition to this correction, it is also possible to actively regulate the temperature of the lens to

a fraction of a degree. For our use, the combination of these two solutions was satisfactory and robust.

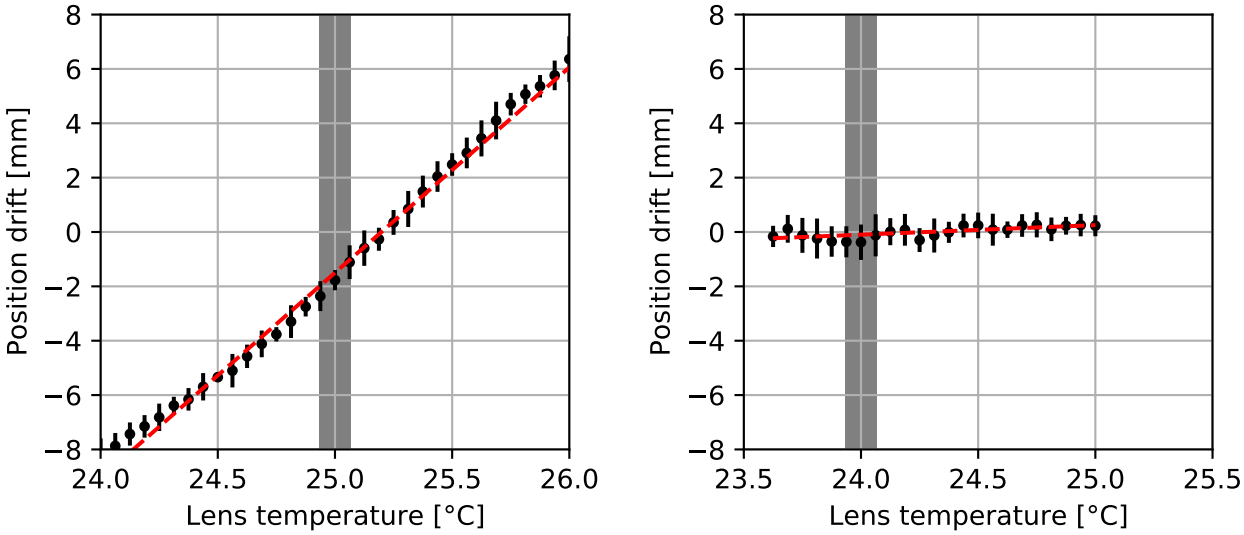

(a) Uncompensated lens. The coil current is held to a constant value during the temperature sweep.

(b) Current compensated lens. The coil current is tuned as the temperature changes in such a way to compensates for the position drift.

Figure 16: Dependence of the trap position with the lens temperature. The grey area indicates the bounds to which it is possible to constrain the temperature when using active regulation.

Another related issue presented itself when the high power laser was used. When the laser is turned on, the center of the lens will start to heat up because a small fraction of the light is absorbed by the fluid. The inhomogeneous temperature gradient in the lens will change its focal length (see fig. 15c). This is often called *thermal lensing*. In our case, the beam remains gaussian, but the position at which the beam is focused changes as the beam heats the lens. It has a drastic effect on the stability of the trap position. Every time the laser is turned on, the trap will jump by a centimetre or more in a couple seconds (see fig. 17a). It is not possible to let the lens reach a steady state because the light must be turned off between every repetition of the experimental sequence.

Fortunately, this effect is also predictable and reproducible. The lens is always heating up and cooling down with the same behaviour depending on the light intensity profile. We can use the same feedforward scheme that is used to compensate the temperature drifts. If the intensity of the laser is known at all times, the drift in the trap position can be predicted by numerically simulating the lens behaviour in real-time with a low pass filter. The expected drift is then compensated by tuning the lens current accordingly (see fig. 17b)[9].

3.3.3 Lens driver

While the flexibility provided by the tunable lens offers precise control of the trap position, correcting for the thermal effects is not straightforward to implement.

[9]This trick can only be applied for reasonably low intensity (large beam size on the lens $w = 3$ mm and low power $P < 10$ W). A discussion with Péter Juhász from Oxford indicates that for larger power ($P = 30$ W) the lens is highly distorted by thermal lensing and the beam no longer has a gaussian profile. This limits the use of this tunable lens to shallow traps where thermal lensing remains a small effect.

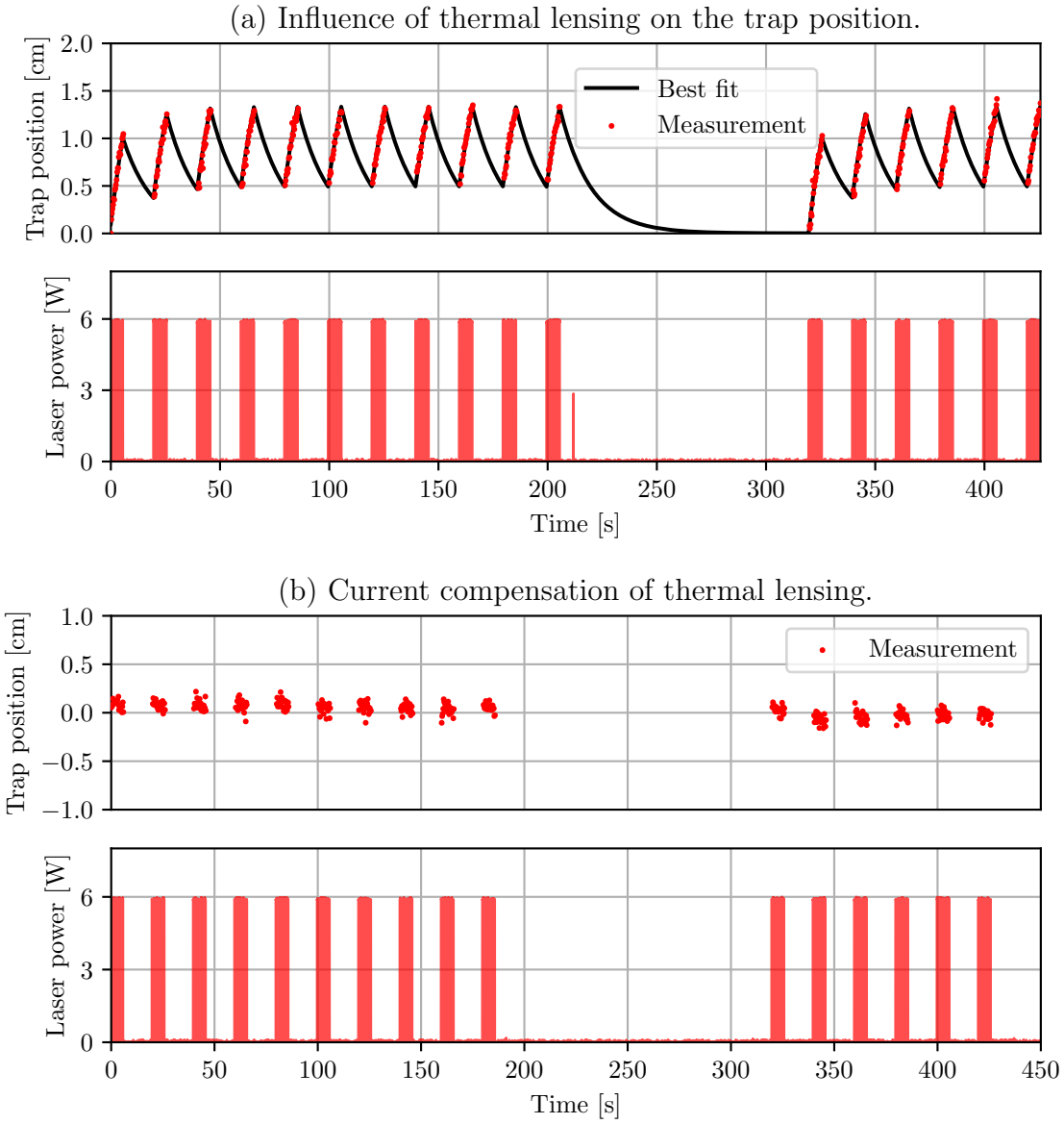

Figure 17: Thermal lensing. The measurements replicate a typical experimental sequence with the high power laser being periodically turned on and off.

In order to simplify the control of the lens for the experiment, I designed an electronic driver[10] that can be used as a black box to provide an accurate control over the position of the trap while hiding the nuisance of the thermal effects compensation.

Below is a quick description of the working principle of the lens driver (see fig. 18). A detailed description of the critical parts and a complete schematic of the system can be found in appendix D.

The tunable lens (1) is tightly encased in an aluminium bloc (2) such that there is good thermal contact between the two parts. With this the temperature fluctuations of the lens is passively reduced.

[10]I designed the lens driver schematic as shown in appendix D, but the routing of the pistes and actual build of the board was done by Dr. Stephen Topliss, electronics technician in the MBQD group.

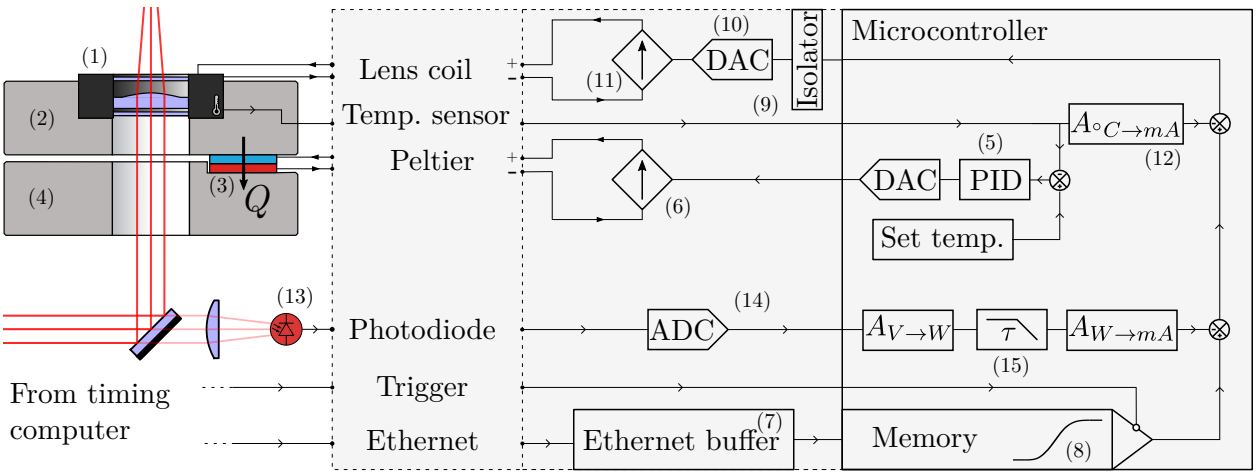

Figure 18: Diagram of the control electronics for the tunable lens.

In addition, the temperature of the lens is actively controlled to remain constant. A peltier module (3) uses an electric current (between ± 2 A) to transfer heat from the bloc (2) to a thermal sink (4). The current flowing through the peltier is generated by a voltage-controlled current source (6). A PID loop (5) reads the lens temperature and adjust the current to try to maintain the temperature.

The current ramp, corresponding to the trap position trajectory, is uploaded via an Ethernet connection (7) to the driver. The digital sequence is stored in the microcontroller memory (8) until a signal triggers the sequence. The digital current is transmitted through a galvanic isolator (9) to a precision digital-to-analogue converter (DAC) (10). The isolator prevents the noise from the microcontroller to be transmitted to the analogue part which would otherwise be transmitted to the atoms. This drives a precision low-noise current source (11) that controls the current in the lens coil and is used to change the curvature of the tunable lens. The lens coil must be driven by a current source and not just by a power voltage source. Indeed, as the lens coil heats up because of the current, its resistance will change, causing the current to change if the voltage was hold constant. This is a different effect than the expansion of the fluid when the lens is hot. It happens in milliseconds and must also be taken into account to have a high control over the trap position.

A digital correction happens in the microcontroller to remove thermal effects that have an undesired influence on the tunable lens. Even if the lens temperature is roughly constant thanks to the PID loop (5), the remaining temperature fluctuations are accounted for by slightly tuning the current to negate the temperature change (12).

The same scheme is used to remove the thermal lensing effect that occurs when a high power beam is shone through the tunable lens. The intensity of the laser is sampled by a photodiode placed behind a back-polished mirror. The intensity of the light is converted to a digital signal and the microcontroller will simulate in real time the effect of the intensity change on the trap position. This is simply done by passing the signal through a low pass numeric filter whose coefficients are chosen to replicate the effect of thermal lensing. The resulting signal is subtracted to the expected trap position to compensate for thermal lensing.

While the driver might seem to complicate the control of the lens, it actually provides transparent control of the trap position to the timing computer in charge of the experiment. With this, it is possible to abstract the tunable lens as a perfect component able to impose arbitrary trajectories to the trap position $z_c(t)$.

4 Transport dynamics

With the technical limitations solved, we can now focus on the physics of transport itself. At the time of writing, it was possible to load the cloud into the transport trap in the cooling chamber. In order to have an enlightened attempt at transport, it is worth investigating some questions concerning its dynamics and see if any prediction can be made to get the best performances from this scheme :

- What is the minimal time for transport with atoms remaining in the trap ?
- Will transport increase the temperature of the cloud ?
- Are there some trajectories for the trap position that are better than others ?

4.1 Harmonic approximation

A simple approach to get a first understanding is to approximate transport dynamics by a single classical particle evolving in a moving harmonic 1D trap :

$$H(t) = \frac{{p_z}^2}{2m} + \frac{m{\omega_z}^2}{2}\left[z - z_c(t)\right]^2 \tag{14}$$

and

$$\dot{z} = \frac{\partial H}{\partial p_z} \qquad \dot{p}_z = -\frac{\partial H}{\partial z} \tag{15}$$

Here z is the position of the particle along the transport axis. p_z is its momentum. $z_c(t)$ is the trap center position, starting in the cooling chamber $z = 0$ at $t = 0$ and arriving in the science chamber $z = D = 50$ cm at $t = t_f$. There is an infinite number of functions $z_c(t)$ satisfying the at the endpoints and we should chose the one that minimises heating and spilling during transport.

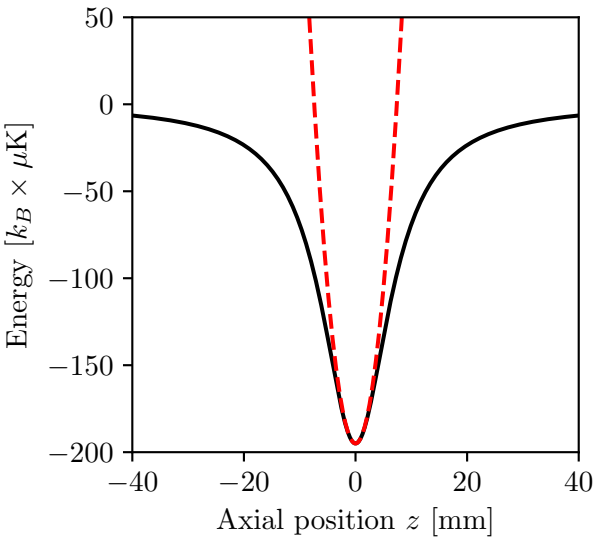

Figure 19: Harmonic approximation (in red) of the true potential (in black).

For a given trap profile $z_c(t)$, it is possible to calculate the energy increase of the particle after transport. It is the amplitude of the Fourier transform of the trap trajectory :

$$\Delta E = H(t_f) - H(0) = \frac{m}{2}{\omega_z}^4 \left| \int_0^{t_f} z_c(t) e^{i\omega_z t} \mathrm{d}t \right|^2 \tag{16}$$

This should be understood as follows : after transport, particles might not be at rest at the trap bottom, but there could be some remaining oscillations around the trap center. If the energy of the oscillations ΔE is larger than the trap depth U_0, there is obviously a problem and the cloud has been lost during transport because the trap was moving too fast for the atoms to follow. Even if $\Delta E < U_0$, this excess energy will be converted to heat through collisions and it will increase the temperature of the cloud. Therefore, there is interest in choosing $z_c(t)$ in order to minimise ΔE.

A first simple solution is *adiabatic transport*. That means moving the atoms so slowly that the cloud stays at the bottom of the trap at all time and and there are no excitations of the cloud motion in the moving referential of the trap. With this approach, the exact profile of the acceleration doesn't matter and it is resilient to experimental imperfections. The question here is, what does *slowly* means and is it compatible with the lifetime of cold atoms in a vacuum chamber ? A simple dimensional analysis tells us that transport is adiabatic when the following condition is fulfilled :

$$t_f > t_{ad} = \frac{2\pi}{\omega_z}\left(\frac{D}{z_R}\right)^{\alpha} \tag{17}$$

Dimensional analysis alone is not able to determine the unknown exponent α. The issue then comes from the large value of D/z_R. For example, with $\alpha = 1/2$, $t_{ad} = 2$ s but for $\alpha = 2$, $t_{ad} = 1200$ s. One value is compatible with experimental conditions, but the other is not.

At this point, it is unclear if adiabatic transport is a good option in our case, but a second solution could allow to bypass condition 17. This method is *non-adiabatic driving* and consists in finding some specific acceleration profiles $z_c(t)$ that don't satisfy the adiabaticity condition but are such that the sum of the phases in ΔE cancels. Such trajectories excite oscillations of the cloud center of mass during transport, but when the motion comes to a stop, the cloud will be remapped to its inital configuration. A variety of theoretical approaches has been considered for harmonic transport where calculations can be fully written down (see for example [TInC+11] for a summary). For the harmonic approximation, it has been shown that ΔE can be cancelled by careful tuning of $z_c(t)$ for any travel distance D and duration t_f.

The issues with this method come when trying to implement it on the experimental side. Equation 16 provides accurate predictions when the trap is close to parabolic [CKRGO08], but in our case, the harmonic approximation seems to be limited (see fig. 19). Trying to take anharmonicity into account for exact calculations can become quickly untractable and provides little to no insights on how to chose optimal trajectories[11].

There is another limitation with this method. Indeed equations 14 and 15 are fully reversible and don't take into account any dissipation in the cloud itself. If the timescale of collisional damping is close to the duration of transport, it could change the predictions made before.

In addition, robustness to experimental unknowns is also an import limiting factor. Maybe we could try to find the perfect trajectory $z_c(t)$ to have no heating, either with careful calculations or by trial-and-error on the experiment. But what would happen is some of the parameters change a bit over time, by a few percents or so ? If the trajectory is over-optimised but not robust to change, it could cause transport to become unreliable over time.

All these reasons might explain why non-adiabatic driving is not a preferred solution for actual experiments, despite its theoretical appeal.

4.2 Transport simulations

4.2.1 Boltzmann equation

The previous harmonic approach fails to give quantitative predictions for the viability of atomic transport in our case. In order to move forward and to have realistic numbers for this situation, a more accurate model needs to be used.

Boltzmann's equation is the tool of choice for this situation as it allows to consider the exact shape of the potential and to take collisional relaxation into account. It has been proven to be a

[11] For example, appendix B of [TInC+11] attempts such a calculation for the optical transport problem.

successful description for cold atoms experiments [WBB11] were quantum effects are not predominant[12].

Boltzmann's equation describes a collection of interacting classical particles which are oscillating in the moving potential of the laser field. It provides a way to evolve the phase-space density function $f(\mathbf{r}, \mathbf{p}, t)$:

$$\frac{\partial f}{\partial t} + \{f, H\} = I_{coll}[f] \tag{18}$$

The second term on the left hand side describes the evolution of particles in the potential of the laser beam :

$$\{f, H\} = \frac{\partial f}{\partial \mathbf{r}} \cdot \frac{\partial H}{\partial \mathbf{p}} - \frac{\partial f}{\partial \mathbf{p}} \cdot \frac{\partial H}{\partial \mathbf{r}} \qquad \text{with} \qquad H(\mathbf{r}, \mathbf{p}, t) = \frac{\mathbf{p}^2}{2m} + U\Big(x, y, z - z_c(t)\Big) \tag{19}$$

This allows the exact form of the potential to be considered, if only to take into account the finite trap depth. Its expression is given by equations 8 and 10.

The term on the right side $I_{coll}[f]$ is the collision operator. An explicit expression can be found in appendix C. It describes how particles at the same position are scattered in and out of their momentum state through collisions. It is necessary to take collisions into account, because the time between two collisions for one particle is of the order of tens of milliseconds, which is small compared to a transport duration of seconds[13].

4.2.2 Numerical simulation

While this equation is a more realistic description of transport, it is no longer possible to perform calculations by hand. In order to get data for transport, I developed a numerical simulation for solving this equation[14]. It uses the Direct Simulation Monte-Carlo method (DSMC) [Bir94]. This technique is close to the real behaviour of atoms in the cloud. It evolves test particles in the potential of the laser and then randomly scatters pairs of particles if they are close enough. These two steps are done for a timestep much smaller than the collision time and can be used for simulating cold atoms. A more detailed description of the method and its implementation for this project can be found in appendix C.

These simulations involve about $10^5 \sim 10^6$ interacting particles and are computationally expensive. This is why I decided to have the code run on graphics processing unit (GPU) using the CUDA toolkit. It allows us to run thousands of independent threads in parallel on the GPU and result in a significant speed-up in this case[15]. Sweeping through an experimental parameter still requires to perform several runs and in this case, calculations were performed on a cluster of 8 GPUs.

To test if these simulations are any use at all for predicting transport behaviour, they were compared to simple situations that can be reproduced experimentally. For example, it is possible to examine the expansion of the cloud in the transport beam after release from the hybrid trap. The initially small cloud will expand in the axial direction and will thermalise in a hundred milliseconds

[12] The system can be described classically because the phase space density $\varpi \sim 10^{-2}$ is much smaller than 1.

[13] The collisional rate for one particle is $\Gamma = n_0 v_{th} \sigma$ where $n_0 \sim 10^{13}$ atoms/cm^3 is the cloud density, $v_{th} = \sqrt{\frac{k_B T}{m}} \sim$20 mm/s is the thermal speed and $\sigma = 8\pi \times (5.7\,\text{nm})^2$ is the cross-section for the collision considered (here *s-wave* for ^{87}Rb)

[14] Complete sources for these simulations are available at https://github.com/damienBloch/cuDSMC.git

[15] From hours per simulation to tens of minutes.

(see fig. 20). The results proved to be in good qualitative agreement with the experiment, even if more care should be taken in determining parameters (atoms number, temperature, ...) in order to get the most accurate results.

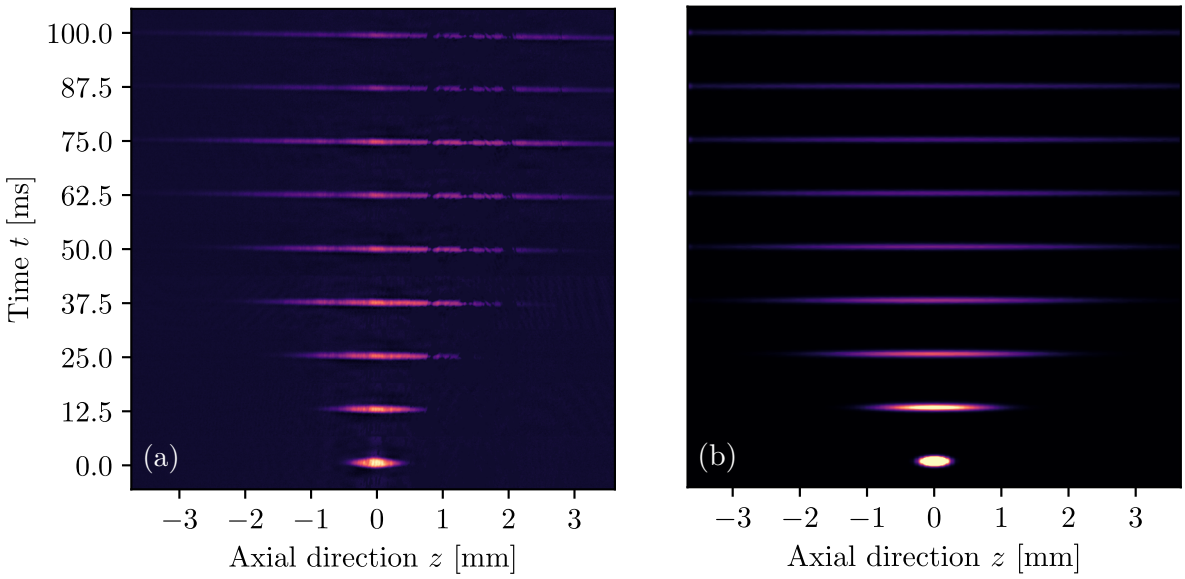

Figure 20: Expansion of the cloud in the transport beam. Each line is a snapshot of the cloud at a different time. (a) Experimental pictures. (b) Simulation of a cloud of 4×10^6 atoms of ^{87}Rb initially at 25 µK. For this data set, the waist is $w_0 = 70$ µm, which explains why the cloud is so large.

These simulations were particularly useful to understand the impact of collisional damping. It severely affects the quadrupole mode of the cloud when its size changes. Instead of a periodic breathing after release from the hybrid trap, the vapour simply expands and thermalises. However, the effect of collisions is reduced for transport itself, because even if the center of mass of the cloud oscillates around the trap center, the relative speed of the atoms doesn't changes and the cloud is always close to a local gaussian equilibrium [goZDS99].

4.2.3 Optimal trajectories

Having a tool that provides realistic numbers, it is also now possible to get answers for the viability of optical transport. For this purpose, I had a look at various acceleration profiles that could be used for transport.

The easiest profile to try from an experimental point of view is just a linear ramp (see fig. 21a). Unfortunately, this gives poor results. It seems that the cloud is lost from the trap if the transport duration is smaller than 5 s. Even for longer ramps, there is substantial heating. This is not too surprising because this kind of ramp involves infinite acceleration at the beginning and the end. At these points, the cloud gets kicked away from the trap center and the oscillations will be converted to heat during transport. Therefore, all the work done during transport will increase the temperature of the cloud.

This is probably the reason why the demonstrating article [LLM+14] opted for smooth trajectories (see fig. 21b) with a finite linear change for the acceleration. In this case, transport timescale becomes viable in 2-3 s with no losses. The energy increase exhibits a more complicated pattern

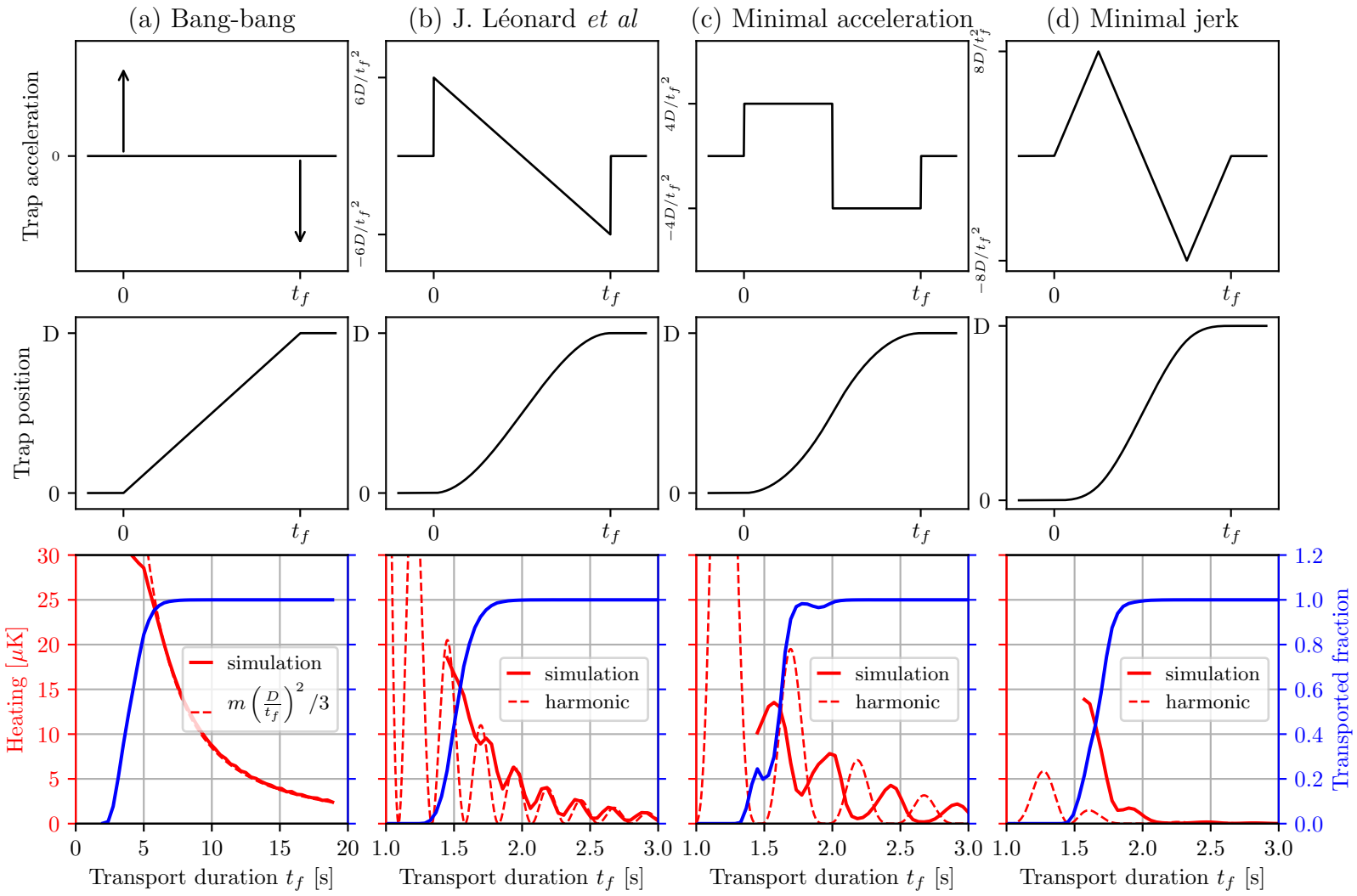

Figure 21: Influence of the shape of the trap trajectory on transport efficiency and heating. Each column contains the results for one specific acceleration profile.

with reminiscence of the harmonic behaviour smeared by the trap anharmonicities and collisional dissipation. This is indeed what Léonard *et al* observed with a similar timescale.

This result is already enough to prove that optical transport is compatible with our expectations. It is still worth trying to see if there is any way to improve on it. For example, maybe a trajectory that minimises acceleration could be better. It would still be smooth but it would reduce the deformation of the trap shape caused by the inertial force $m\ddot{z}_c(t)$. The results can be seen on fig. 21c and are similar to the previous ones. The predictions made by the harmonic approximation are qualitatively correct. However, their predictive power is limited and the exact pattern for the temperature highly depends of the exact trap shape.

More interesting is to minimise the jerk $\dddot{z}_c(t)$ that indicates the rate of change of the trap shape due to the inertial force (see fig. 21d). This way the trap change is continuous in time. The cloud

remains at the instantaneous trap bottom at all times and no dynamics are induced. As can be seen, it is not detrimental to the timescale for transport but removes the ripples in the energy increase for durations larger than 2 s. This approach is also resilient to small changes in the system and doesn't strongly depend of the exact shape of the potential or of the trajectory. It appears that it could be a satisfactory solution for the problem considered.

The last trajectory seems to be fairly similar to the definition of adiabatic transport. It is also quite surprising that trajectory 21d is adiabatic for durations t_f larger than 3 s, but that trajectory trajectory 21a is not, even for t_f larger than 20 s.

4.3 Adiabatic transport

The previous results can be summarised by having a proper definition for adiabaticity in the case of harmonic transport. A possible definition is :

> *The evolution of a system is adiabatic if there are no energy excitations ($\Delta E \ll U_0$) when the change applied to the system is slow compared to its dynamics ($t_f \gg 1/\omega_z$).*

Let us apply this definition to expression 16. For this purpose, only the behaviour of the decaying envelope of ΔE for large t_f matters and the exact shape of the oscillations is not taken into account.

The Paley-Wiener theorem relates the decay of the Fourier transform of $z_c(t)$ when $\omega_z \to \infty$ to the *smoothness* of $z_c(t)$. Let us define n to be the smallest integer such that $\frac{\mathrm{d}^n z_c}{\mathrm{d}t^n}$ presents a discontinuity. This is the number of times it is possible to derive $z_c(t)$ without issues. For example, $n = 1$ for trajectory (a), $n = 2$ for (b) and (c), and $n = 3$ for (d). With this, the Paley-Wiener theorem states :

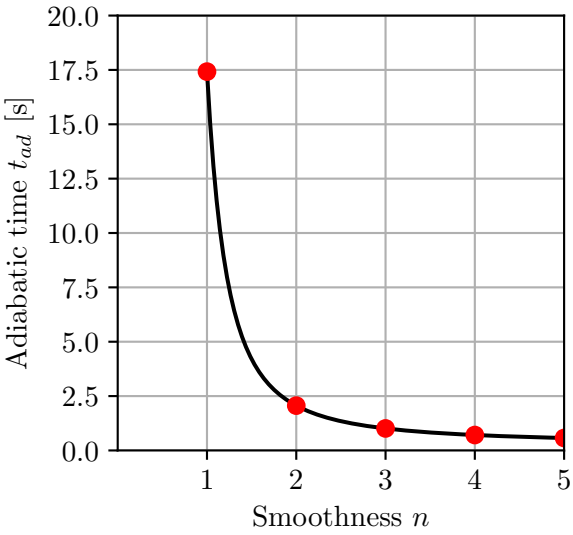

Figure 22: Evolution of the adiabatic time t_{ad} depending on the smoothness of the trajectory for the experiment considered.

$$\left| \int_0^{t_f} z_c(t) e^{i\omega_z t} \mathrm{d}t \right| < \frac{t_f}{{\omega_z}^n} \max \left| \frac{\mathrm{d}^n z_c}{\mathrm{d}t^n} \right| \quad \text{as} \quad \omega_z \to \infty \tag{20}$$

For slowly changing trajectories, a reasonable value for $\frac{\mathrm{d}^n z_c}{\mathrm{d}t^n}$ is $\frac{D}{{t_f}^n}$ and we can replace this in the previous expression. Putting everything together in the adiabatic condition $\Delta E \ll U_0$ yields the explicit adiabatic condition for t_f :

$$t_f > t_{ad} = \frac{2\pi}{\omega_z} \left(\frac{D}{z_R} \right)^{\frac{1}{n}} \tag{21}$$

The adiabatic timescale for optical transport depends on the *smoothness* n of the trajectory considered. t_{ad} is plotted in figure 22 for our trap parameters.

With this, it is possible to understand the previous results. For $n = 1$, t_{ad} is large, of the order of several tens of seconds. But when n is increased to 2, the coefficient $(D/z_R)^{\frac{1}{n}}$ is not so large and

adiabatic transport is suddenly a viable option for us. Increasing n to 3 still gives some benefits, but nowhere comparable as before. For even larger values of n, t_{ad} quickly levels off to $2\pi/\omega_z$ and there is not much point trying to go for larger values of n.

This indicates that adiabatic transport is a satisfactory solution for the Kagome experiment, assuming that the trajectory is smooth enough. With this it should be possible to transport a cold cloud of atoms overs 50 cm with virtually no change in atom number or temperature increase.

Conclusion

The aim of this project was to implement a protocol of optical transport for cold atoms with a tunable lens and to test its viability in regards to the conditions imposed by the Kagome experiment in the MBQD group.

The technical scheme itself if fairly simple and elegant. It gives the possibility to highly control the position of an atomic cloud by changing the focus of a red-detuned dipole beam in which the atoms are trapped. The central component is a tunable lens that can achieve large displacement in short times and with no moving mechanical pieces. However, the main technical limitations also come from the lens itself. Indeed, thermal effects affecting the lens can cause the trap position to drift over time in an unacceptable range. Fortunately, these effects are always reproducible. It is therefore possible to predict them in advance and use feed-forward techniques to reduce them to a tolerable level.

Regardless of the actual implementation, a major question that needed answering is how fast atoms can be transported without spilling out of the trap or being heated. A careful analysis of the condition for adiabaticity in a harmonic trap shows that it highly depends on the smoothness of the acceleration profile. When the trap trajectory is highly regular, the cloud can indeed be displaced by several tens of centimetres in a couple of seconds, which is acceptable. This theoretical prediction was also compared to a more realistic approach. Using numerical simulations it is possible to incorporate complicated real-life effects like collisions of finite-trap depth. The results of the calculations validate the previous hypothesis and confirm that optical transport can be successfully applied to this experiment.

Because of the covid-19 situation, it was not possible to fully complete the project and actually transport a cloud to the science chamber. The next steps in this regards will be to compare the predictions made to experimental data and test transport over large distances. It would be particularly interesting to see if the shape of the trajectory has such a large influence on the performance of transport.

References

[AEM+95] M. H. Anderson, J. R. Ensher, M. R. Matthews, C. E. Wieman, and E. A. Cornell. Observation of bose-einstein condensation in a dilute atomic vapor. *Science*, 269(5221):198–201, 1995.

[BGP+09] Waseem S. Bakr, Jonathon I. Gillen, Amy Peng, Simon Fölling, and Markus Greiner. A quantum gas microscope for detecting single atoms in a hubbard-regime optical lattice. *Nature*, 462(7269):74–77, Nov 2009.

[Bir94] G. A. Bird. *Molecular Gas Dynamics And The Direct Simulation Of Gas Flows*. 1994.

[Blo05] Immanuel Bloch. Ultracold quantum gases in optical lattices. *Nature Physics*, 1(1):23–30, Oct 2005.

[BML00] V I Balykin, V G Minogin, and V S Letokhov. Electromagnetic trapping of cold atoms. *Reports on Progress in Physics*, 63(9):1429–1510, aug 2000.

[CKRGO08] A. Couvert, T. Kawalec, G. Reinaudi, and D. Guéry-Odelin. Optimal transport of ultracold atoms in the non-adiabatic regime. *EPL (Europhysics Letters)*, 83(1):13001, jun 2008.

[DJ99] B. DeMarco and D. S. Jin. Onset of fermi degeneracy in a trapped atomic gas. *Science*, 285(5434):1703–1706, 1999.

[Fey82] Richard P Feynman. Simulating physics with computers. *International journal of theoretical physics*, 21(6/7):467–488, 1982.

[Foo07] Christopher J Foot. *Atomic physics*. Oxford master series in atomic, optical and laser physics. Oxford University Press, Oxford, 2007.

[Gol14] M.J. Goldsworthy. A gpu–cuda based direct simulation monte carlo algorithm for real gas flows. *Computers & Fluids*, 94:58 – 68, 2014.

[goZDS99] David guéry odelin, Francesca Zambelli, Jean Dalibard, and Sandro Stringari. Collective oscillations of a classical gas confined in harmonic traps. *Physical Review A*, 60, 04 1999.

[GWO00] Rudolf Grimm, Matthias Weidemüller, and Yurii B. Ovchinnikov. Optical dipole traps for neutral atoms. volume 42 of *Advances In Atomic, Molecular, and Optical Physics*, pages 95 – 170. Academic Press, 2000.

[HA10] Sebastian D. Huber and Ehud Altman. Bose condensation in flat bands. *Phys. Rev. B*, 82:184502, Nov 2010.

[JGT+12] Gyu-Boong Jo, Jennie Guzman, Claire K. Thomas, Pavan Hosur, Ashvin Vishwanath, and Dan M. Stamper-Kurn. Ultracold atoms in a tunable optical kagome lattice. *Phys. Rev. Lett.*, 108:045305, Jan 2012.

[JZ05] D. Jaksch and P. Zoller. The cold atom hubbard toolbox. *Annals of Physics*, 315(1):52 – 79, 2005. Special Issue.

[LLH+17] Jun-Ru Li, Jeongwon Lee, Wujie Huang, Sean Burchesky, Boris Shteynas, Furkan Çağrı Top, Alan O. Jamison, and Wolfgang Ketterle. A stripe phase with supersolid properties in spin–orbit-coupled bose–einstein condensates. *Nature*, 543(7643):91–94, Mar 2017.

[LLM+14] Julian Léonard, Moonjoo Lee, Andrea Morales, Thomas M Karg, Tilman Esslinger, and Tobias Donner. Optical transport and manipulation of an ultracold atomic cloud using focus-tunable lenses. *New Journal of Physics*, 16(9):093028, sep 2014.

[LMZ+17] Julian Léonard, Andrea Morales, Philip Zupancic, Tilman Esslinger, and Tobias Donner. Supersolid formation in a quantum gas breaking a continuous translational symmetry. *Nature*, 543(7643):87–90, Mar 2017.

[LPC+09] Y.-J. Lin, A. R. Perry, R. L. Compton, I. B. Spielman, and J. V. Porto. Rapid production of ^{87}Rb bose-einstein condensates in a combined magnetic and optical potential. *Phys. Rev. A*, 79:063631, Jun 2009.

[Sie86] Anthony E. Siegman. *Lasers*. University Science Books, 1986.

[SOT97] T. A. Savard, K. M. O'Hara, and J. E. Thomas. Laser-noise-induced heating in far-off resonance optical traps. *Phys. Rev. A*, 56:R1095–R1098, Aug 1997.

[TInC+11] E. Torrontegui, S. Ibáñez, Xi Chen, A. Ruschhaupt, D. Guéry-Odelin, and J. G. Muga. Fast atomic transport without vibrational heating. *Phys. Rev. A*, 83:013415, Jan 2011.

[WBB11] A. Wade, D. Baillie, and P. Blakie. Direct simulation monte carlo method for cold atom dynamics: classical boltzmann equation in the quantum collision regime. *Physical Review A - PHYS REV A*, 84, 05 2011.

[YHW11] Simeng Yan, David A. Huse, and Steven R. White. Spin-liquid ground state of the s = 1/2 kagome heisenberg antiferromagnet. *Science*, 332(6034):1173–1176, 2011.

[ZS97] Meiqing Zhang and Robert D. Skeel. Cheap implicit symplectic integrators. *Applied Numerical Mathematics*, 25(2):297 – 302, 1997. Special Issue on Time Integration.

A Kagome band structure

Even if solving the full Hubbard Hamiltonians is too difficult, one can expect that they have an interesting behaviour based on the non-interacting picture, *i.e.* when only considering hoping between sites in the tight-binding model.

To calculate the band structure of the Kagome lattice for single particle, it is useful to define the vector (resp. its hermitian conjugate)

$$\widehat{\mathbf{b}}_{i,j} = \begin{bmatrix} \hat{b}_{i,j,A} \\ \hat{b}_{i,j,B} \\ \hat{b}_{i,j,C} \end{bmatrix} \tag{22}$$

which annihilates (resp. creates) a particle on the sites A,B or C of the primitive cell located at $\mathbf{R}_{i,j} = i\,\mathbf{a}_1 + j\,\mathbf{a}_2$.

With this, the tight-binding Hamiltonian can be simply expressed by looking at the adjacency of the sites :

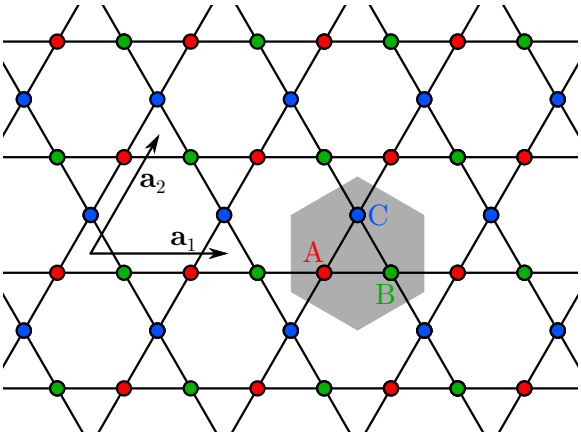

Figure 23: Kagome geometry with its lattice vectors $\mathbf{a}_1$, $\mathbf{a}_2$ and the basis sites A, B, and C in each unit cell (gray).

$$\begin{aligned}\widehat{H}_{TB} = -t \sum_{i,j} \widehat{\mathbf{b}}^\dagger_{i,j} \begin{bmatrix} 0 & 1 & 1 \\ 0 & 0 & 1 \\ 0 & 0 & 0 \end{bmatrix} \widehat{\mathbf{b}}_{i,j} + \widehat{\mathbf{b}}^\dagger_{i-1,j} \begin{bmatrix} 0 & 0 & 0 \\ 1 & 0 & 0 \\ 0 & 0 & 0 \end{bmatrix} \widehat{\mathbf{b}}_{i,j} \\ + \widehat{\mathbf{b}}^\dagger_{i,j-1} \begin{bmatrix} 0 & 0 & 0 \\ 0 & 0 & 0 \\ 1 & 0 & 0 \end{bmatrix} \widehat{\mathbf{b}}_{i,j} + \widehat{\mathbf{b}}^\dagger_{i+1,j-1} \begin{bmatrix} 0 & 0 & 0 \\ 0 & 0 & 0 \\ 0 & 1 & 0 \end{bmatrix} \widehat{\mathbf{b}}_{i,j} + \text{h.c.}\end{aligned} \tag{23}$$

Having defined this, a useful tool is its reciprocal representation in the Brillouin zone :

$$\widehat{\mathbf{b}}_{\mathbf{k}} = \frac{1}{\sqrt{N}} \sum_{i,j} e^{i\mathbf{k}\cdot\mathbf{R}_{i,j}}\, \widehat{\mathbf{b}}_{i,j} \qquad \text{and} \qquad \widehat{\mathbf{b}}_{i,j} = \frac{1}{\sqrt{N}} \sum_{B.Z.} e^{-i\mathbf{k}\cdot\mathbf{R}_{i,j}}\, \widehat{\mathbf{b}}_{\mathbf{k}} \tag{24}$$

Converting to the pseudo-momentum representation by replacing $\widehat{\mathbf{b}}_{i,j}$ with the expression above, the Hamiltonian has a much simpler form that is now straightforward to diagonalize :

$$\widehat{H}_{TB} = -t \sum_{B.Z.} \widehat{\mathbf{b}}^\dagger_{\mathbf{k}} \begin{bmatrix} 0 & 1 + e^{i\mathbf{k}\cdot\mathbf{a}_1} & 1 + e^{i\mathbf{k}\cdot\mathbf{a}_2} \\ 1 + e^{-i\mathbf{k}\cdot\mathbf{a}_1} & 0 & 1 + e^{i\mathbf{k}\cdot(\mathbf{a}_1 - \mathbf{a}_2)} \\ 1 + e^{-i\mathbf{k}\cdot\mathbf{a}_2} & 1 + e^{-i\mathbf{k}\cdot(\mathbf{a}_1 - \mathbf{a}_2)} & 0 \end{bmatrix} \widehat{\mathbf{b}}_{\mathbf{k}} \tag{25}$$

The three energy bands are the eigenvalues of the previous matrix :

$$E_0(\mathbf{k}) = 2t \tag{26}$$

$$E_\pm(\mathbf{k}) = -t \left(1 \pm \sqrt{3 + 2\left[\cos(\mathbf{k}\cdot\mathbf{a}_1) + \cos(\mathbf{k}\cdot(\mathbf{a}_1 - \mathbf{a}_2)) + \cos(\mathbf{k}\cdot\mathbf{a}_2)\right]}\right) \tag{27}$$

B ABCD matrices calculations

Paraxial gaussian optic can be described using the formalism of ABCD matrices. With this approach, the electric field of a gaussian beam is parametrised as follow :

$$E(x,z) = \Re\left(e^{-i\pi x^2/q(z)\lambda} e^{i(\omega t - kz)}\right) \tag{28}$$

Here $q(z)$ is the complex beam parameter :

$$\frac{1}{q(z)} = \frac{1}{R(z)} - \frac{i\lambda}{\pi w(z)^2} \tag{29}$$

with $R(z)$ the curvature at the beam at a point z of the optical axis and $w(z)$ is the beam transverse size. $q(z)$ contains all the information to describe a gaussian beam.

The advantage of this formulation is that it is easy to propagate the beam parameter through an arbitrary optical system described by a matrix ABCD. If the beam parameter at the input of the system is q_1, the beam parameter at the output is :

$$q_2 = \frac{Aq_1 + B}{Cq_1 + D} \tag{30}$$

The ABCD matrix of a system is the product of the matrices of its constitutional components. For example, the matrices for propagation in free-space by a distance d or through a lens of focal length f are respectively :

$$\Pi(d) = \begin{bmatrix} 1 & d \\ 0 & 1 \end{bmatrix} \quad \text{and} \quad \Lambda(f) = \begin{bmatrix} 1 & 0 \\ -1/f & 1 \end{bmatrix} \tag{31}$$

This can be applied to the optical transport scheme. It is described in section 3.1 and simply consists of the tunable lens of optical power p followed by a fixed lens of focal length f at distance d. To show that this setup should behave as expected, we can calculate the ABCD matrix of this system :

$$M = \Lambda(f)\Pi(d)\Lambda(1/p) \tag{32}$$

Once this is done, we know the trap waist w_0 for an incoming collimated beam of size w_i :

$$w_0 = \sqrt{\frac{f^2\lambda^2 {w_i}^2}{\lambda^2(d-f)^2 + \pi^2 {w_i}^4[1 + p(f-d)]^2}} \tag{33}$$

In order for w_0 to be independent of the optical power p of the focus tunable lens, we must have $d = f$ and in which case we indeed have :

$$w_0 = \frac{\lambda f}{\pi w_i} \quad \text{and} \quad z_c = f(2 - fp) \tag{34}$$

The trap at the position z_c can be translated in block without having its shape changed.

C Direct Simulation Monte-Carlo

C.1 Method overview

This section is a brief summary of the Direct Simulation Monte-Carlo (DSMC) calculations. More details about the method or its implementation can be found for example in [Bir94], [Gol14] or [WBB11]. This technique is used as a numerical approximation to Boltzmann equation :

$$\frac{\partial f}{\partial t} + \{f, H\} = I_{coll}[f] \tag{35}$$

The term on the left is described in section 4.2.1. $I_{coll}[f]$ is the collision operator which can be written down as :

$$I_{coll}[f](\mathbf{p}_1) = \frac{\sigma}{m} \int \mathrm{d}^3\mathbf{p}_2 \int \mathrm{d}^2\mathbf{\Omega} |\mathbf{p}_1 - \mathbf{p}_2| \left[f(\mathbf{r}, \mathbf{p}_1^*) f(\mathbf{r}, \mathbf{p}_2^*) - f(\mathbf{r}, \mathbf{p}_1) f(\mathbf{r}, \mathbf{p}_2) \right] \tag{36}$$

It describes how two particles of momentum $\mathbf{p}_1$ and $\mathbf{p}_2$ and at the same position are scattered to end up in momentum $\mathbf{p}_1^*$ and $\mathbf{p}_2^*$. The new momenta are constrained by total momentum and energy conservation. These relations can be parametrised with $\mathbf{\Omega}$, the solid angle formed by the incoming and outgoing relative momenta. Here only *s-wave* collisions are considered for ^{87}Rb as higher order collisions are prohibited at low temperature. $\sigma = 8\pi {a_0}^2$ is the cross-section with a scattering length $a_0 = 5.7$ nm.

A mathematical treatment of this operator is cumbersome and the numerical implementation can in some sense be easier to understand. It consists in approximating the continuous phase-space density $f(\mathbf{r}, \mathbf{p}, t)$ by a set of N_T particles of position $\mathbf{r}_i(t)$ and momentum $\mathbf{p}_i(t)$:

$$f(\mathbf{r}, \mathbf{p}, t) \simeq \alpha \sum_{i=1}^{N_T} \delta\left(\mathbf{r} - \mathbf{r}_i(t)\right) \delta\left(\mathbf{p} - \mathbf{p}_i(t)\right) \tag{37}$$

Here $\alpha = N_P / N_T$ is the number of physical particles N_P per simulation particle. The method differs from molecular dynamics as there can be several atoms (here between 10∼100) per test particle.

For each timestep, the particles are evolved according to the external potential and also undergo collisions.

C.2 Advection

One step in the DSMC method is to move the particles according to the potential of the laser. This is were parallel architecture particularly shines as each particle can be simulated independently of the others. For each particle that consists in solving Hamilton equations for a small timestep Δt :

$$\frac{\mathrm{d}\mathbf{r}_i}{\mathrm{d}t} = \frac{\mathbf{p}_i}{m} \qquad\qquad \frac{\mathrm{d}\mathbf{p}_i}{\mathrm{d}t} = \mathbf{F}(\mathbf{r}_i, t) \tag{38}$$

This is a common numeric problem, but there are some difficulties that comes from the shape of the trapping potential. We only care about the dynamics on the timescale of the transport and the axial frequency ($\sim$ 5 Hz). However there is a strong force on a much smaller timescale ($\sim$ 800 Hz) in the radial direction. This is known as a stiff problem : the timestep must be much smaller than the minimal timescale for explicit integration, which is prohibitive. One way to solve this is with the following method [ZS97] :

$$\mathbf{r}_i^{n+1/2} = \mathbf{r}_i^n + \frac{\Delta t}{2}\frac{\mathbf{p}_i^n}{m} \tag{39}$$

$$\dot{\mathbf{p}}_i^{n+1/2} = \mathbf{F}\left(\mathbf{r}_i^{n+1/2} + \lambda\,\Delta t^2\,\frac{\dot{\mathbf{p}}_i^{n+1/2}}{m}\right) \tag{40}$$

$$\mathbf{p}_i^{n+1} = \mathbf{p}_i^n + \Delta t\,\dot{\mathbf{p}}_i^{n+1/2} \tag{41}$$

$$\mathbf{r}_i^{n+1} = \mathbf{r}_i^{n+1/2} + \frac{\Delta t}{2}\frac{\mathbf{p}_i^{n+1}}{m} \tag{42}$$

This method is symmetric in time and if there is no time dependence in the force, it conserves energy, which is crucial in this case. The second step is an implicit equation for $\lambda \neq 0$ and is solved with a couple iterations of Newton method. It allows to consider a larger timestep Δt that would otherwise be unstable for explicit methods.

C.3 Collision

The characteristic step for the DSMC technique is the collisions handling. For this, space is discretised in cells containing only a couple tens of particles each. See for example figure 24 were the atom density is higher in the center of the crossed dipole trap, requiring a smaller grid size.

Then each cell is assumed to have an uniform density and will treat the collisions for the particles it contains. For one cell of volume ΔV, the probability for two particles i, j to collide is :

$$P_{i,j} = \alpha\sigma\frac{\Delta t|\mathbf{p}_i - \mathbf{p}_j|}{\Delta V m} \tag{43}$$

Each couple of particles (i, j) in the cell is randomly tried for collisions with probability $P_{i,j}$. If a collision is accepted, the momenta of the particles is evolved as follow :

$$\mathbf{p}_i \to \frac{\mathbf{p}_i + \mathbf{p}_j}{2} + \mathbf{\Omega}\frac{|\mathbf{p}_i - \mathbf{p}_j|}{2} \tag{44}$$

$$\mathbf{p}_j \to \frac{\mathbf{p}_i + \mathbf{p}_j}{2} - \mathbf{\Omega}\frac{|\mathbf{p}_i - \mathbf{p}_j|}{2} \tag{45}$$

where $\mathbf{\Omega}$ is a random unit vector.

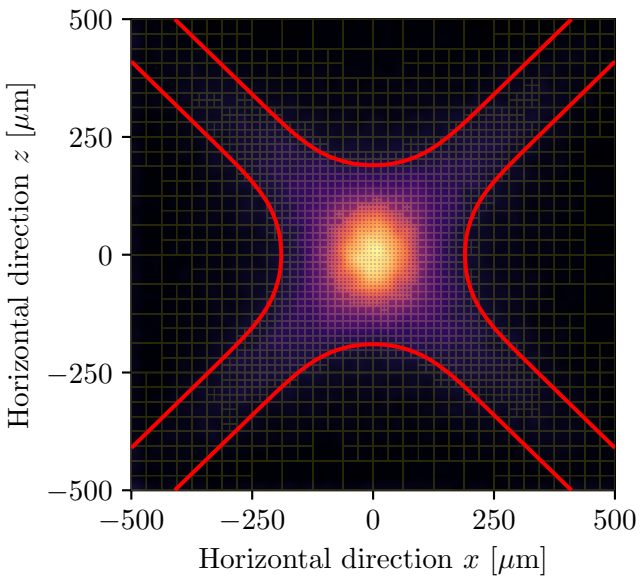

Figure 24: Simulated evaporation in the crossed dipole trap. Atoms are more likely to leave the trap along the arms were the depth is lower.

For a large number of particles, this step is an approximate solution to the evolution $\frac{\partial f}{\partial t} = I_{coll}[f]$ for hard-sphere collisions.

Concerning the actual parallel implementation, the particle array is sorted using a z-ordering curve such that it is easy to access the particles contained in each cell. A grid of blocks corresponding to the spatial grid is launched. Each block will load the momenta of its particles in fast shared memory so that threads can perform collision calculations without having to access global memory.

While the adaptive grid might seem to be ill-suited for parallel architectures, for the situations considered, it was not the bottleneck with only about 30% of the total time. The rest of the simulation is spent evolving particles in the external potential.

D Lens driver

In this appendix, some details about the lens driver circuits are summarized.

D.1 Basic current source

Besides the microcontroller, there are also two current sources. These parts are easy to build with discrete components and this approach gives more flexibility than with built-in parts. The current source (6)[16] for the peltier module needs a symmetric output between ±2 A. There is no particular specification for noise or accuracy, therefore it is readily implemented with the circuit from figure 25.

It consists of a high current operational amplificator (OPA548) that sets its output such that the potential difference between its two inputs is null. In order for this to be true, the voltage drop developed on a sense resistor R_S (1 Ω, 25 W) needs to be the same as the command voltage V_I. Because the sense resistor is in serie with the load R_L (here the Peltier module) and the inverting input of the op amp doesn't draw any current, the same current is going through R_S and R_L.

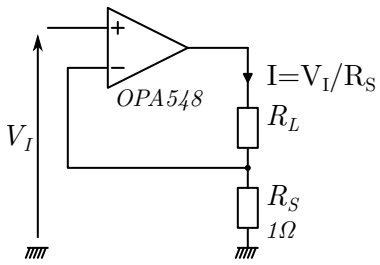

Figure 25: Basic current source

While being really simple, this current source works quite well and provides a current that is accurate to the milliampere scale. This kind of accuracy is however not enough for the current source (11) driving the lens coil because a change of $1\,mA$ corresponds to a position change of about $6\,mm$.
There are several reasons for this error in the current. The op amp used needs to have a high output current, but this comes with a large input offset voltage drift and a high voltage noise. Also the sense resistance R_S changes with temperature which would cause the current to drift after a prolonged use. One last issue is that there is a voltage difference between the ground to which V_I is measured and the return ground for the current I to which the voltage drop over R_S is measured. This difference is due to the high return current that induces IR voltage drop in the traces it is going through. All these factors adds up to limit the precision reached on the current and need to be corrected for the current source driving the lens coil.

[16] Numbers refer to figure 18.

D.2 Precision current source

Improving on the previous design, it is possible to build a current source that is suitable to control the tunable lens (see fig. 26).

DAC

The DAC converter for controlling the current source is an external integrate component U_1 that is isolated from most of the noise form the microcontroller by a galvanic isolation U_2. This allows to have two different grounds, an analogue GND_2 and a digital one GND_1. Therefore it doesn't matter if the digital ground has some voltage jumps when the microcontroller switches its outputs.

The microcontroller U_1 is a precision 16 bits DAC. It outputs a voltage $V_{OUT} = V_{REF} \times D/2^{16}$, where D is a 16bits digital signal transmitted from the microcontroller and V_{REF} is a $+2.5V$ reference from an external regulator U_3. The input impedance for the reference voltage and the ground of the DAC depends of the output voltage that is asked. To prevent this from having a negative influence on the DAC precision, the $+2.5V$ reference voltage and the ground reference are buffered with op-amps U_4 and U_5.

The DAC output voltage is buffered and symmetrised in the range $\pm 2.5V$ with an external op-amp U_6. C_2 and C_3 are just here to low-pass filter the output with a critical frequency of 1kHz. This op-amp produces a command voltage V_I that is used to drive the analogue current source.

Current source

This current source can be understand as a PID controller (PI^2 in this case) with a transfer function $A = A_1 A_2$. This controller forms a feedback loop when it is closed with an element β that measures the current going through the tunable lens coil. This way, the control element $A_1 A_2$ outputs whatever is needed to set the difference between the control voltage V_I and the output of β to 0.

In the β block, the current is again measured by placing a sense resistor R_S in serie with the lens. In this case however, R_S is a precision power resistor (Y092610R0000T9L) with a low temp coefficient. The voltage drop is measured with an instrumentation amplifier U_9 (INA821). The negative lead of the in-amp is on the high side of R_S to have an overall negative feedback when the loop is closed. The A_1 and A_2 blocks act as one effective op-amp. It can provide high output current with the power op-amp U_8 at the output, but it also has low noise and drift when it is placed in a feedback loop because the input is a high precision op-amp U_7. This way, only the noise from U_7 and U_9 matters and this can be made low.

Frequency response

One complication is the frequency dependence of the feedback network when we look at the time response of the system. The DC behaviour can be understood by ignoring the components C_4 , C_5 , R_5 and R_8. However, if they are removed, the inductance of the lens coil L_{OPT} will form a low pass filter and create a resonance with the active parts. This will cause the circuit to behave as an oscillator, which is obviously unwanted. This problem happens if a sine wave of frequency ω is amplified by a factor greater and gets a phase shift of 180° after going through the amplifier $A_1 A_2$ and the return network β. To prevent this, the open loop gain $A_1(\omega)A_2(\omega)\beta(\omega)$ must have a modulus smaller than 1 when the phase shift is higher than 180°. This is a theoretic criteria and a rule of thumb for stability in practice, is that the gain $|A_1 A_2 \beta|$ must be smaller than 1 when the

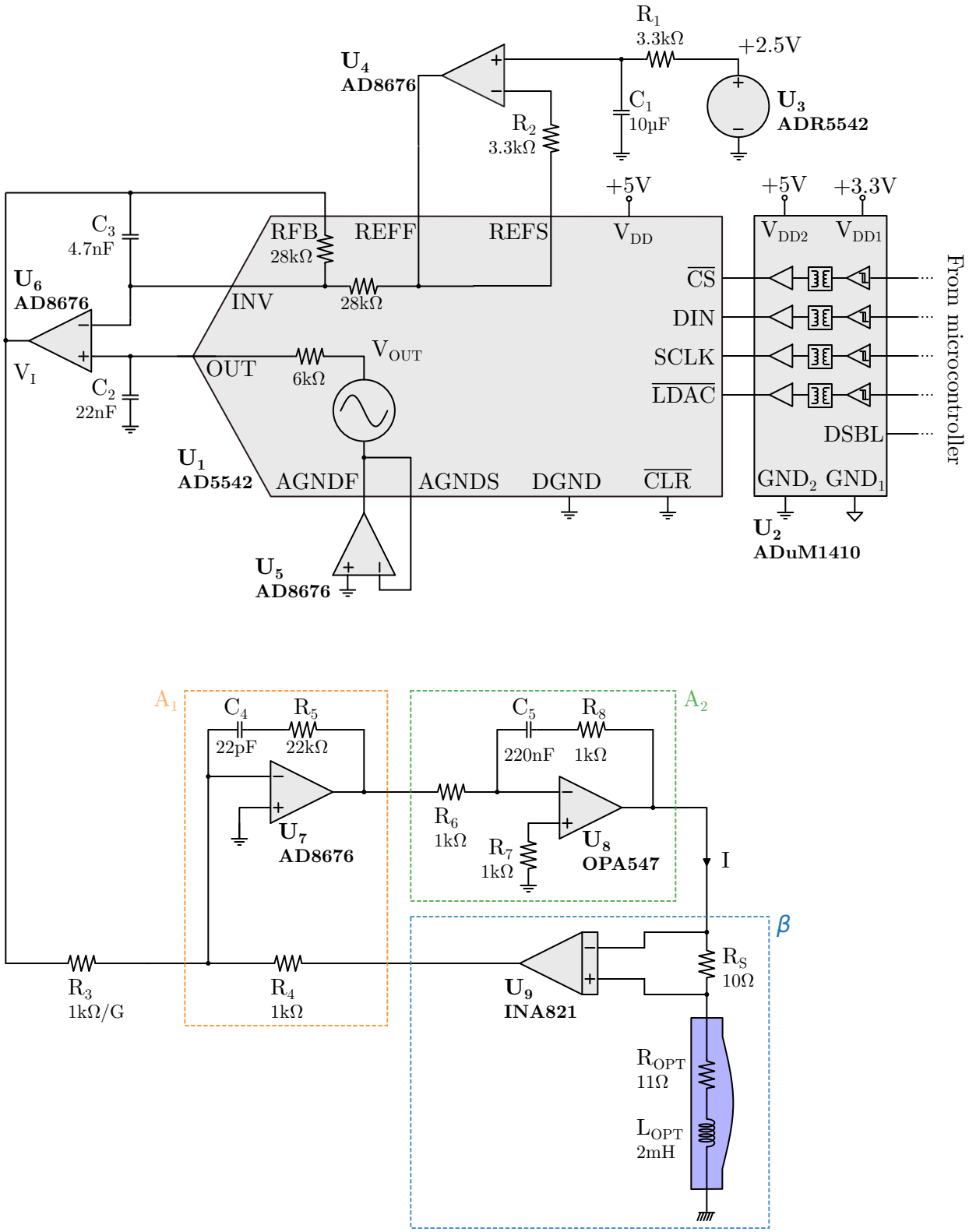

Figure 26: Improved current source

phase shift is higher than 145°. This gives a bit a room to accommodate for the unknowns in a real circuit. Furthermore this criteria has a nice graphical interpretation : in a Bode plot, the $1/\beta$ gain must cross the A_1A_2 curve with a 20dB/decade rolloff.

Figure 27 is the Bode plot of the open-loop response of the circuit. The op-amp U_7 and U_8 behaves each as a PI controller so A_1A_2 is a PI^2 controller with reaction feedback adjusted so that the blue and red curves cross at 20dB/decade. The tick lines are piecewise approximations that I used to calculate C_4, C_5, R_5, R_8 to have the desired behaviour and the dashed lines are SPICE simulations.

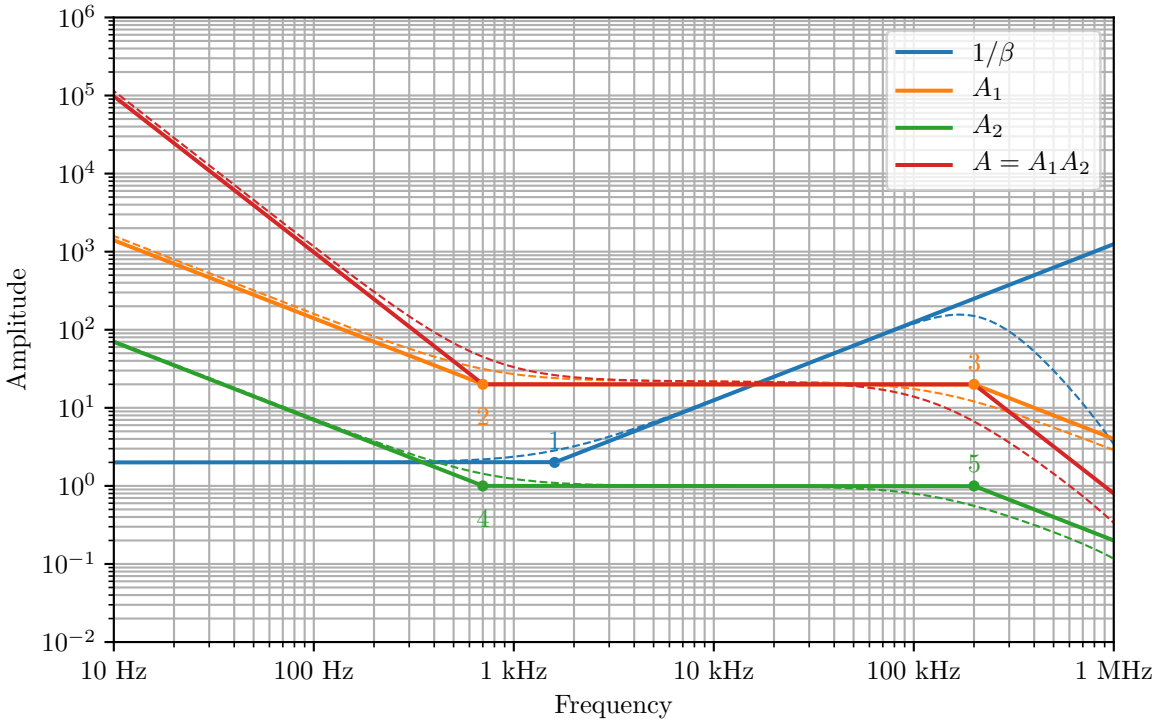

Figure 27: Open-loop Bode diagram of the current source

D.3 Schematic